Published in final edited form as:
NMR Biomed. 2011 July ; 24(6): 734–749. doi:10.1002/nbm.1669.

Assessment of therapeutic response and treatment planning for brain tumors using metabolic and physiological MRI

Sarah J. Nelson[a,*]
[a]University of California at San Francisco – Mission Bay, San Francisco, CA, USA

Abstract

MRI is routinely used for diagnosis, treatment planning and assessment of response to therapy for patients with glioma. Gliomas are spatially heterogeneous and infiltrative lesions that are quite variable in terms of their response to therapy. Patients classified as having low-grade histology have a median overall survival of 7 years or more, but need to be monitored carefully to make sure that their tumor does not upgrade to a more malignant phenotype. Patients with the most aggressive grade IV histology have a median overall survival of 12–15 months and often undergo multiple surgeries and adjuvant therapies in an attempt to control their disease. Despite improvements in the spatial resolution and sensitivity of anatomic images, there remain considerable ambiguities in the interpretation of changes in the size of the gadolinium-enhancing lesion on T_1-weighted images as a measure of treatment response, and in differentiating between treatment effects and infiltrating tumor within the larger T_2 lesion. The planning of focal therapies, such as surgery, radiation and targeted drug delivery, as well as a more reliable assessment of the response to therapy, would benefit considerably from the integration of metabolic and physiological imaging techniques into routine clinical MR examinations. Advanced methods that have been shown to provide valuable data for patients with glioma are diffusion, perfusion and spectroscopic imaging. Multiparametric examinations that include the acquisition of such data are able to assess tumor cellularity, hypoxia, disruption of normal tissue architecture, changes in vascular density and vessel permeability, in addition to the standard measures of changes in the volume of enhancing and nonenhancing anatomic lesions. This is particularly critical for the interpretation of the results of Phase I and Phase II clinical trials of novel therapies, which are increasingly including agents that are designed to have anti-angiogenic and anti-proliferative properties as opposed to having a direct effect on tumor cell viability.

Keywords

brain tumors; diffusion; perfusion; MRS; therapeutic response

INTRODUCTION

Gliomas are the most common type of primary brain tumor in adults and originate from the support cells of the brain or neuroglia. The World Health Organization (WHO II) definition of the severity or grade of these lesions (1–4) is based on the degree of malignancy or aggressiveness that is observed in microscopic analysis of biopsy or surgical samples. Criteria that are considered include the level of invasiveness, similarity to normal cells, growth rate and presence of abnormal vascularity (5–8). Grade I tumors are slow growing

[*]Correspondence to: S. J. Nelson, University of California at San Francisco –Mission Bay, Byers Hall, Room BH-303, MC 2532, 1700 4th Street, San Francisco, CA 94158-2330, USA. sarah.nelson@radiology.ucsf.edu.

and are considered to be benign. Grade II tumors are deemed low grade, but exhibit nuclear atypia and can progress if left untreated. Depending on the cell of origin, they may be termed astrocytoma, oligodendroglioma or of mixed type. Grade III tumors have mitotic figures in addition to nuclear atypia, and the most common subtype is anaplastic astrocytoma because of its higher cellularity and increased vascularity. Grade IV gliomas, or glioblastoma multiforme (GBM), are defined by the existence of regions of necrosis, higher cellularity, increased vascularity and proliferation. Although these histological criteria are well defined, the heterogeneity and infiltrative nature of these tumors mean that biopsy or surgical resection is not always accurate, and samples from the same patient may be classified as corresponding to more than one grade. In such cases, the diagnosis corresponding to the highest observed grade is the one that is used.

The availability of noninvasive MR technologies for the assessment of the location and spatial extent of the lesion is a critical factor in making decisions about the management of patients with glioma. The presence of regions with abnormal microvasculature causes breakdown of the blood–brain barrier (BBB) in grade IV and some grade III gliomas, which appears as regions of contrast enhancement on post-gadolinium T_1-weighted images (see Fig. 1). Regions of necrosis are common for grade IV glioma and may be observed as central areas of hypointense signal on such images. Surrounding regions of infiltrative tumor and edema exhibit hyperintensity on T_2-weighted images and typically extend over a much larger region of the brain. Grade II and some grade III lesions show reduced or normal vasculature and appear as nonenhancing on post-gadolinium T_1-weighted images. The situation becomes more complex after therapy as treatment-induced changes may mimic tumor progression in both enhancing and nonenhancing abnormalities. Grade II lesions may become contrast enhancing, and it is difficult to determine from standard imaging criteria alone whether they have transformed to a higher grade (9–12). It is for this reason that recent studies have investigated the use of more advanced imaging methods that are able to monitor physiological and metabolic properties of the tumor and surrounding tissue.

The purpose of this review is to examine recent results that have been obtained with MR diffusion-weighted, perfusion-weighted and metabolic imaging, and to discuss how they should be used in treatment planning and the assessment of treatment response. The integration of such information into clinical practice is a priority, both in terms of tailoring therapy to individual patient characteristics and for use as surrogate markers of biological effects in clinical trials. Although some standardization is needed in terms of implementing the advanced imaging sequences required to acquire such data in a uniform manner across all scanner platforms, there is beginning to be a consensus on which parameters are of interest, and several cooperative groups are poised to demonstrate their clinical value in a multi-institutional setting.

TREATMENT AND ASSESSMENT OF RESPONSE TO THERAPY

As shown in Fig. 2, imaging plays a critical role in all aspects of the management of patients with glioma. The primary treatment for all grades is surgical resection with the goal of removing as much of the tumor as possible, whilst having a minimal effect on neurological function. Even in cases in which the surgeon feels that there is gross total resection, there is typically residual malignant disease and recurrence occurs close to or at the site of the original lesion (13). Imaging plays a critical role in all aspects of treatment after maximal safe resection; patients with grade III and grade IV glioma receive fractionated radiation therapy (RT) to the residual anatomic lesion and a further 2–3-cm margin (14). Although some reports have indicated that higher doses are effective in reducing tumor burden, the formation of extensive necrosis and the impact on surrounding normal tissue mean that the standard dose used for fractionated external beam radiation is usually 2 Gy/day, with a total

of 60 Gy being delivered to the primary target (15–21). Chemotherapies are widely applied in an adjuvant setting, both for residual disease and at the time of recurrence, but have traditionally shown limited effectiveness (22). Much of this is thought to be a result of the difficulty in delivery to portions of the tumor because of the effects of BBB. The recent use of temozolomide, which is given concurrently and as an adjuvant to RT, has improved survival in patients with high-grade glioma (23,24) and is increasingly being applied in patients with low-grade glioma (25–28). For patients with grade II glioma who have undergone gross total resection, the treatment varies between institutions and, in many cases, further therapy is delayed until there are signs of tumor progression. The outcome differs between tumor subtype, with grade II oligodendroglioma being more likely to respond to chemotherapy than grade II astrocytomas (29–31).

If clinical and radiological assessment of the patient indicates that there is recurrent tumor, the options include further surgical resection (32), focal radiation with advanced delivery methods, such as gamma knife radiosurgery or cyberknife (33), chemotherapy with standard agents or the use of investigational approaches that currently include immunotherapy (34) and convection-enhanced delivery of novel agents (35–37). The definition of tumor burden and the ability to plan focal therapy are significantly compromised by the ambiguities inherent inconventional T_1- and T_2-weighted images. Pseudo-progression, which is defined as an increase in the enhancing volume of the tumor that occurs without any associated clinical symptoms and disappears on subsequent scans without a change in therapy, is increasingly being identified as a concern (38–45). A further complication for patients with grade II glioma is that the tumor may recur with the characteristics of a high-grade lesion that requires more aggressive treatment in order to have an impact on the course of the disease. The availability of noninvasive imaging methods that can more reliably differentiate between upgraded and nonupgraded lesions, as well as distinguishing between recurrent tumor and treatment effects (46), is critical for making decisions about patient care.

In the case of anti-angiogenic agents in which therapy acts via a mechanism that influences the permeability of BBB, there is also the possibility of observing the phenomenon of pseudo-response, which corresponds to a reduction in enhancement on T_1-weighted images without an effect on tumor cell viability. This is of particular concern in the case of anti-angiogenic agents such as Bevacizumab (47–51), which has recently received provisional Food and Drug Administration (FDA) approval for the treatment of patients with recurrent high-grade glioma. Although dramatic initial responses have been reported with agents that act via a similar mechanism in terms of the restoration of normal vasculature, there appears to be a higher frequency of distant as opposed to local failure that is thought to correspond to an increase in the infiltrative nature of the lesion (52,53). Although these effects are still being evaluated and are not fully understood, the proposed solution is to combine this treatment with agents with other modes of action that have complementary effects (54–60). Of critical importance in the assessment of the response to such combination therapies is therefore the availability of techniques that can directly and objectively assess not only changes in vascular density and vessel permeability (36–39), but also more directly monitor changes in tumor cell viability. Although novel therapeutic approaches have been shown to extend survival in patients with glioma by a few months, there is plenty of room for improvement, and the evaluation of new combination therapies is essential.

The field of neuro-oncology is cognizant of the limitations in evaluating the effects of therapy using conventional MRI methods (61,62). The Macdonald criteria for the assessment of the radiological response for patients with brain tumors are a specialized version of the Response Evaluation Criteria In Solid Tumors (RECIST) and are based on changes in the size of the gadolinium-enhancing anatomic lesion (61). As indicated previously, even for cases in which there are unambiguous regions of enhancement within

the larger T_2 lesion (T2L), these changes are confusing for the evaluation of therapeutic agents with anti-angiogenic activity (42–46) and for those that inhibit signaling pathways rather than causing direct cytotoxic effects (49,50). The accurate determination of the efficacy of conventional and novel agents requires new methods for the assessment of changes in the biological properties of the lesion. A recent initiative from the neuro-oncology community defined modified Response Assessment in Neuro-Oncology (RANO) criteria for the evaluation of the response for patients with GBM (63). These take into account changes in fluid-attenuated inversion recovery (FLAIR) or T_2-weighted MR images, as well as post-gadolinium T_1-weighted images. Although this is a promising start, the definition of the standard lacks quantitative rigor and does not yet include findings from more advanced MR physiological and metabolic imaging methods.

UTILITY OF DIFFUSION-WEIGHTED MRI

The ability to measure the diffusion properties of water using MRI opens up the possibility to assess changes in tissue architecture associated with a variety of different disease processes (64–66). The addition of diffusion gradients to widely available echo planar imaging techniques has allowed for the estimation of parameters that reflect both the magnitude and directionality of diffusive processes with good spatial resolution and minimal motion problems. Quantitative parameters that can be estimated when applying gradients in multiple spatial directions are the apparent diffusion coefficient (ADC) and the fractional anisotropy (FA). The acquisition time for diffusion-weighted imaging from the brain with six-directional weighting is of the order of 2–6 min, and with 55 or more gradient directions, typically used to calculate the connectivity of white matter tracts, is of the order of 10–15 min at clinical field strengths. For patients with brain tumors, ADC has been proposed as a measure of tumor cellularity (66) and FA as a means to assess the disruption of normal white matter caused by degenerative processes. For cases in which diffusion-weighted images are acquired with six or more gradient directions, some researchers have also analyzed maps of the individual eignenvalues of the estimated diffusion tensor (EV1, EV2 and EV3). The use of a large number of diffusion gradient directions is critical for performing tractography (67,68), which is employed for surgical planning, in terms of defining how the presence of a lesion has disrupted the connectivity of different regions of the brain and has distorted the location of different brain structures that are critical for the maintenance of normal function.

Recent studies of data from patients with glioma have suggested that variations in ADC within the anatomic lesion are able to distinguish between different histological subtypes for grade II glioma (69–71), as well as differentiating between upgraded and nonupgraded recurrent low-grade glioma and predicting clinical outcome for patients with grade IV glioma (72). To quantify such differences, the most common method is to draw regions of interest (ROIs) on the anatomic images and look at intensity variations in maps of ADC and FA. The regions considered are typically normal-appearing white matter (NAWM), the overall T2L and the contrast-enhanced lesion (CEL). In some cases, there are also regions of hypointensity on T_1-weighted images that are thought to correspond to necrosis (NEC). Superimposing such ROIs on the aligned ADC, FA, EV1, EV2 and EV3 maps allows for the generation of histograms of intensity values in each ROI and an analysis of descriptive parameters, such as the 10th percentile, 25th percentile, median, mode, skewness and kurtosis. If the sequences are properly calibrated, these should be absolute measures of diffusion. It is also convenient to scale the estimated parameters by median value in NAWM. This can be determined by the segmentation of white and gray matter, or by looking at the mode (position of the peak) in the histogram of the ADC intensities in the entire brain. In our experience, the use of such normalized diffusion parameters removes some of the variability observed between scanners of different field strengths, software

versions and manufacturers. Another alternative would be to use an externally calibrated phantom for quality control (73).

The first critical thing to note in the evaluation of ADC values in different tumor ROIs is that the majority of values attributable to tumor are higher than in NAWM. If the tumor infiltrates into normal tissue and there is a heterogeneous mixture of both types of cell within the same voxel, the interpretation of changes in ADC values becomes more complex. Necrosis and edema both have relatively high ADC. For untreated grade II oligodendromas, the median ADC in T2L is around 1.6 times that in NAWM and, for untreated grade II astrocytomas, the median intensity is 1.8–1.9 times that of NAWM (72). This difference is thought to be a result of the manner in which astrocytomas infiltrate into normal brain, which causes a more extensive breakdown of the tissue architecture. Figure 3 shows a method for highlighting the presence of regions within these tumor subtypes using color coding of ADC values, which not only provides a noninvasive prediction of histology, but may also be important for the characterization of lesions of mixed subtype (70). If these color images are imported into the surgical navigation workstation and viewed during resection, it is easy to highlight which areas of the lesion should be chosen for taking samples to perform histological analysis.

The median ADC values for grade III and grade IV gliomas are approximately 1.5 times that of NAWM within T2L, with a trend towards lower values in CEL (72). An analysis of the prognosis for 56 patients with untreated grade IV glioma showed that both the pre-surgical values of the 10th percentile of ADC in CEL and the volume of the overall T2L that exhibited ADC values less than 1.5 times that of NAWM were predictive of shorter overall survival (74). These results are consistent with other published data (75–77) and with the notion that the presence of regions with ADC values in the range of 1.0–1.5 times that of NAWM in CEL of grade IV glioma are associated with a more cellular and aggressive phenotype.

Immediately after surgery there are often regions of very low ADC close to the cavity that subsequently become enhancing and then disappear in follow-up examinations. In a recent analysis of 32 patients with grade IV glioma who had pre-surgical, immediate post-surgical and pre-RT MR examinations, it was found that 21 of 32 patients showed reduced diffusion and eight subsequently exhibited increased enhancement within a similar region that could have been confused with tumor progression (78). This implies that the inclusion of diffusion-weighted imaging in the immediate post-surgical scan may be helpful in distinguishing between real and pseudo-progression. It is also interesting to note that, when the pre-RT examination was taken as the new baseline scan for an expanded cohort of patients with grade IV glioma, both the volume of T2L and the volume within T2L that showed ADC less than 1.5 times that of NAWM were predictors of poor overall survival, but the volume of CEL was not (79).

The interpretation of changes in ADC becomes even more complex following RT and adjuvant chemotherapy (80,81) because of treatment-induced gliosis, necrosis and edema. One strategy that has been proposed to make an early prediction of whether a patient is responding to therapy is the use of the functional diffusion map (fDM), which makes direct correlations on a pixel-by-pixel basis of ADC values within an ROI spanning the overlapping CELs from pre-RT *versus* mid-RT scans (82–89). The number of pixels for which values have changed significantly (either increased or decreased) compared with the overall overlapping lesion volume has been proposed as a predictor of both radiological response and overall survival. This method requires that there is a residual CEL and that the algorithm used to register images between the pre-RT and mid-RT scans is able to match the pixels accurately. The authors of these papers proposed that there must be a residual CEL of

4 cm^3 in size for the analysis to be effective. In our experience, this is often not the case for newly diagnosed gliomas in surgically accessible locations and, with the dramatic reductions in CEL seen with anti-angiogenic agents, the size of the common region that can be studied may be further compromised. An alternative strategy may be to consider an ROI defined by the residual T2L or from the region that is metabolically abnormal.

Our early results in comparing ADC values in CEL and T2Ls in cohorts of patients with grade IV glioma treated with different types of anti-angiogenic agent have indicated that there are clear differences in the pattern of changes from pre-RT to mid-RT and post-RT scans that may provide information about the manner in which the agent is acting (90). It should be noted that the mid-RT scan is not routinely obtained for clinical purposes, and thus further research is required to determine whether the current findings can justify the performance of an extra scan.

For the long-term assessment of changes in ADC for high- and low-grade gliomas, the analysis of changes in parameters that describe the shape of the histogram has been proposed. For patients with grade IV glioma undergoing treatment with Bevacizumab, Pope *et al*. (91) fitted the histogram of ADC intensities in CEL with a sum of two Gaussian functions, and found that smaller values of mean ADC for the lower component were predictive of a poor outcome. In our analysis of serial changes in the median and 10th percentile of ADC values in the anatomic lesions of patients with grade IV glioma treated with RT and temozolomide without anti-angiogenic agents, we found, in a time-dependent analysis, that these did not predict progression-free survival, but did predict overall survival (92). One reason for this may be the observation that median ADC values in new areas of enhancement for patients with grade IV glioma typically increase prior to recurrence, and are substantially higher than could be interpreted as being a result of increased cellularity. This is consistent with the concept that changes in the value of ADC in such lesions reflect a complex combination of effects caused by the disruption of normal tissue, treatment-induced necrosis, edema and infiltrative tumor.

Tozer *et al*. (93) examined 27 patients with low-grade glioma who were being followed with watchful waiting as opposed to receiving any treatment. They found that the ADC for oligodendrogliomas was less than for astrocytomas, and that ADC decreased on malignant progression. Our evaluation of patients with an original diagnosis of grade II glioma, who were scheduled for surgery because of suspected recurrence, showed that there were clear differences in the median ADC values for individuals whose lesions had upgraded to grade III or grade IV histology compared with those who did not upgrade. A similar result was found by the analysis of ADC values at locations corresponding to image-guided tissue samples that were obtained during surgery. The upgraded tissue samples showed higher tumor cellularity score and higher MIB-1. Another interesting observation was that the ADC values for the nonupgraded grade II oligodendroglioma were higher than the values obtained for the newly diagnosed, untreated lesion (94). This is consistent with the interpretation of such changes as being caused by a treatment effect, but highlights the complexities inherent in the analysis of such data.

In summary, there are a number of factors that decrease the ADC values observed in gliomas. These include increased tumor cellularity, increasing tumor grade, histology corresponding to untreated grade II oligodendroglioma, reduction in edema caused by the use of steroids and partial voluming of tumor with NAWM. Factors that increase the ADC values observed in glioma include the disruption of normal tissue architecture, gliosis, treatment effects and edema. Hence, although ADC is a useful adjunct to anatomic imaging and may help to provide quantitative parameters for the characterization of lesion characteristics, the interpretation of changes in ADC that occur in response to therapy must

consider carefully the tumor grade, type of therapy applied and steroid usage. Future work should seek to perform a more detailed analysis of changes in FA and the magnitude of eigenvalues (EV1, EV2 and EV3) to determine whether these parameters will provide an extra dimension that may help to distinguish between treatment effects and recurrent tumor (73).

ASSESSMENT OF VASCULAR PROPERTIES

A number of MRI techniques have been applied to assess changes in microvasculature and to link variations in the estimated parameters with response to therapy (95–103). The two methods most commonly used in the brain are dynamic contrast-enhanced (DCE) and dynamic susceptibility-weighted contrast (DSC) imaging. Recent reviews have provided a thorough description of the methodology and examples of patient data (104–106). Briefly, DCE imaging takes advantage of the changes in T_1 associated with the passage of gadolinium through the vasculature and leakage into the extracellular space for regions in which BBB has been compromised (107–111). When applying rapid *k*-space sampling techniques in conjunction with the latest parallel reconstruction strategies, a time resolution of 5–10 s can be achieved for a three-dimensional imaging sequence that covers an axial slab of 6–8 cm. A number of different approaches have been applied to analyze the changes in signal intensity from these dynamic data and to estimate parameters such as the fractional blood volume (fBV) and permeability (K_{ps} or K_{trans}). The most widely used model is from Tofts and Kermode (111).

DSC imaging uses echo planar sequences with a rapid bolus of gadolinium to assess changes in T_2^*within the vasculature and interstitial space with a 1–2-s time resolution (95). The change in relaxivity is estimated as being proportional to the concentration of gadolinium, which is assumed to be represented by $C(t)$, which is proportional to $-\ln[S(t)/S_0)]/\mathrm{TE}$, where $S(t)$ is the signal intensity at time t, S_0 is the initial intensity and TE is the echo time. This transformation changes the decrease in the observed signal intensity, which corresponds to the arrival of the agent in the local vasculature, to an increase in the estimated concentration $C(t)$. The changes in intensity are typically characterized by the peak height (PH), area under the curve relative to NAWM (relative cerebral blood volume, rCBV) and the percentage recovery (%REC) or recirculation factor (RF). For situations in which BBB has broken down, the leakage of gadolinium into the interstitial space requires the use of a more complex nonlinear function to fit the concentration–time curve (112–115). The effect observed represents a balance between the changes in T_1 and T_2^*, and is influenced by the flip angle of the excitation pulse and the vessel permeability. A recent study examined a number of different acquisition parameters and analysis methods for patients with high-grade glioma (115). It concluded that either a dual echo sequence that could separate the T_1 and T_2^* effects of the contrast agent, or the use of a pre-dose of gadolinium that was able to reduce the impact of the disruption of BBB on the estimation of rCBV, was valuable for analyzing the changes in signal intensity.

Parametric maps that are derived from DCE and DSC imaging data have been proposed as noninvasive methods for predicting the tumor grade (97,116–118) and assessing the response to therapy (119,120). Grade II astrocytomas have fBV and rCBV that are iso- or hypointense with NAWM and relatively low permeability (118). Grade II oligodendrogliomas may exhibit diffuse enhancement and typically have moderate intensity on the corresponding maps of fBV and rCBV (69,72). Although 50–60% of grade III gliomas exhibit some degree of enhancement, their vascularity and permeability are intermediate in value. Increased vasculature is present in both enhancing and nonenhancing components of grade IV glioma (103). As illustrated by the data from the patient in Fig. 4, the dynamic curves are flat in regions of necrosis, but there are high peak values in the

enhancing rim and reduced recovery in the lateral and anterior edge of the tumor. Although the presence of abnormal vasculature is known to be a histologically characteristic marker for grade IV glioma, the magnitude and spatial extent of elevated rCBV in the initial pre-surgery scan were not found to be predictive of overall survival (74). One explanation for this is that, because the surgical resection is focused on the enhancing volume, it typically removes the majority of the region with increased vasculature. Figure 5 shows an example of a gross total resection of an untreated grade IV glioma and illustrates what a dramatic difference surgery can make.

For patients with a residual vascular abnormality, conventional treatment with RT and temozolomide exhibits a short-term effect on the lesion, with a reduction in rCBV and a temporary increase in permeability. The magnitudes of these changes are reflected in the size of CEL, with the lesion on the post-RT scan representing a balance between the two effects. Cases in which there is increased permeability may result in increased delivery of temozolomide to the target and hence a greater chance of causing DNA damage. This is one explanation for pseudo-progression. Although regions in which rCBV is reduced may show worse drug delivery, the compromised vasculature may result in lower oxygenation that acts to enhance the damaging effect of RT. How these short-term effects impact on the overall effectiveness of the treatment is difficult to predict, and further work is required to examine the link between temporal changes in vasculature and outcome. In a recent study that followed a cohort of patients with grade IV glioma through their initial treatment, it was found that, although there was an association between progression-free survival and rCBV at pre-RT and post-RT examinations, none of the vascular parameters were related to overall survival (92). Obtaining complementary data that examine the effect of treatment on metabolic or other tumor cell parameters may be helpful in understanding the relationship between short-term changes in vasculature and long-term effects on the lesion as a whole.

The ability to monitor changes in permeability and vascular density is expected to be critically important for the assessment of the impact of anti-angiogenic agents. In such cases, there is an ongoing debate as to the most appropriate time points to detect the effect on MR parameters, and whether DCE or DSC techniques should be used to evaluate such changes. Although many research studies have been able to acquire both types of data in the same MR examination, increasing concerns about the influence of higher doses of gadolinium on patients with compromised kidney function mean that patients are less enthusiastic about participating in such studies. Batchelor *et al.* (119) performed a detailed analysis in order to assess the normalization of vasculature in patients with recurrent GBM who were receiving adjuvant AZD2171 at time periods ranging from 1 to 112 days after treatment using a combination of DCE and dual-echo DSC methods. They observed rapid functional vascular normalization, as measured by a reduction in vessel size and overall permeability, which was found to be reversible when the drug was temporarily removed from the treatment regimen. The changes in vascular parameters were combined with differences in circulating collagen IV levels between pre-therapy and 1-day post-therapy to create a ‘vascular normalization index’ that was found to be predictive of both overall and progression-free survival (119). Future studies will examine how these parameters evolve during the full course of therapy for patients with newly diagnosed GBM, and will perform a more detailed analysis of how they relate to radiographic response and clinical outcome.

One such study that is nearing completion at our institution has applied DSC imaging to examine changes in tumor vasculature during the first 2 months of therapy for patients with GBM being treated with RT, temozolomide and enzastaurin (121). Analysis of the data showed that patients who exhibited a large decrease in PH after 1 month of therapy and improvement in %REC after 2 months of therapy had a more favorable response. The level of recovery present at the end of this period was also found to be predictive of progression-

free survival. These results support the hypothesis that DSC imaging provides information about changes in vascular function during therapy that may ultimately aid clinicians to identify patients who are likely to benefit from such therapy and demonstrate an early indicator of response. One concern in using changes in the size of CEL as the gold standard for the assessment of response to anti-angiogenic therapies is that the amount of gadolinium leakage is a reflection of the vascular density and permeability, as opposed to being an independent measure of the reduction in tumor burden. Continued follow-up is required to assess the relationship of these changes to overall survival and to determine whether there are variations in the patterns of response for agents that act via different mechanisms.

The use of high-resolution susceptibility-weighted imaging (SWI) techniques emphasizes the contrast of the magnitude image by applying a mask that is derived from the phase data to visualize changes in vascular parameters for patients with brain tumors, followed by a minimum intensity projection to emphasize venous structures. The transition of routine clinical neuroimaging examinations from 1.5 to 3 T has provided the opportunity to significantly improve the quality of such images. In addition to highlighting increased vasculature in the region of the tumor, it is possible to detect the presence of small hemorrhages that are associated with radiation damage within regions of normal brain tissue (122,123). Our group has taken further advantage of the increase in susceptibility effects at high field in order to provide high-resolution SWI data at 7 T. Although it is unlikely that this will be adopted for routine clinical examinations, the increased sensitivity that it provides has helped us to observe some very dramatic effects. Of interest is the fact that the formation of hemorrhages is specific to RT as opposed to chemotherapy, and that the delay in appearance of hemorrhages is typically 2–3 years. The ability to quantify the location and impact of such late radiation effects in normal brain tissue may be important for planning treatment margins in patients with low-grade glioma, who may otherwise develop treatment-induced neurocognitive deficits.

MR METABOLIC IMAGING

The first observations that used ^{1}H MRS to detect differences in metabolite levels between normal brain and tumor were performed over 15 years ago (124–133). Parameters that are observed in the brain at a moderate echo time of 144 ms and that provide insight into changes associated with tumor progression include levels of choline-containing compounds (Cho), creatine (Cr), *N*-acetylaspartate (NAA), lactate (Lac) and lipid (Lip). The intensity of the Cho signal reflects changes in membrane synthesis and turnover that are associated with cell proliferation and remodeling. The Cr peak is often used as a reference for normalizing the intensity of other metabolites, and includes both creatine and phosphocreatine. NAA is a marker of normal brain tissue that is typically assumed to correspond to the presence of actively functioning neurons. Lac is an end-product of anaerobic metabolism and may therefore reflect ischemia and/or hypoxia. In cases in which there has been care to avoid artifacts caused by inadequate suppression of the signal from subcutaneous Lip, the presence of Lip peaks is interpreted as being a result of necrosis.

Single-voxel ^{1}H MRS with either point-resolved spectroscopy (PRESS) or stimulated echo acquisition mode (STEAM) localization is typically applied with a voxel size of 4–8 cm^3 and an acquisition time of 2–5 min (128). MRSI provides a two- or three-dimensional array of spectra from 1–2-cm^3 voxels and may use PRESS localization from a much larger selected volume or a slice selection and spin echo sequence (131). Additional Lip suppression is typically achieved with spatially selective saturation pulses and/or an inversion pulse that nulls out these signals. At the field strength of 3 T, with a multichannel radiofrequency coil and a combination of phase encoding and echo planar sampling, it is possible to routinely obtain a 16 × 16 × 16 array of spectra from the brain with a nominal

voxel size of 1 cm^3 in 5–10 min (134–136). Parallel imaging strategies can further cut down the acquisition time or increase coverage, but the signal-to-noise ratio is a limiting factor (137,138). Although most scanners have automated shim routines, regions close to the sinuses and brainstem may still give poor quality spectra.

Numerous studies have shown that brain tumors are characterized by an increase in Cho and decrease in NAA relative to normal (139–142), and that the changes in these metabolites are more sensitive to the detection of infiltration and residual disease than is gadolinium-enhanced MRI. This is particularly important for planning and assessing the response to radiation and other focal therapies (143–150). An example is shown in Fig. 6, where the shaded voxels that have high Cho and low NAA are seen to extend far beyond CEL. To more accurately describe the metabolic lesion and make visual comparisons with the anatomic lesion, we have defined a *z* score that is termed the Cho to NAA index (CNI), and have used it to quantify the difference between tumor and normal (151). Color maps of the CNI or contours of regions with CNI greater than two or greater than three can then be superimposed on the anatomic images to represent the spatial extent of the lesion. It should be noted, however, that there are treatment effects on metabolism in normal brain (152–154), and there are other disease processes, such as inflammation, that can cause a reduction in neuronal function and an increase in cellularity. This means that abnormal CNI should be viewed as defining the spatial extent of abnormal metabolism, and is consistent with, rather than specific for, the tumor.

Other parameters of interest that provide useful information and can add to the specificity of CNI are the levels of Lac and Lip. With an echo time of 144 ms, the Lac peak is inverted and its presence in the tumor can be used to infer the likelihood of it being high rather than low grade. Lip peaks are at a similar frequency and may be present in grade IV glioma, even when there is no obvious area of necrosis in the anatomic images. The use of a Lac editing pulse sequence is important to avoid the signals from these peaks cancelling each other out and to unambiguously distinguish between them (155). *In vivo* MRS with shorter echo time (TE =30–40 ms) and recent studies using *ex vivo* MRS have indicated that levels of myo-inositol/Cho may also be valuable for separating low-grade from high-grade glioma and in distinguishing gliosis from recurrent grade IV glioma (156–158). Tissue and preclinical studies have also confirmed that phosphocholine (PC) represents the predominant contribution to the *in vivo* Cho peak in grade IV glioma, whereas glycerophosphocholine (GPC) is the major component in grade II glioma (94). Previous studies using ^{31}P MRSI have also demonstrated differential changes in PC and GPC in response to therapy, but the spatial resolution of 4–8 cm^3 that can be obtained at clinical field strengths requires improvement.

The fact that there is abnormal metabolism in the non-enhancing region of the tumor means that it can be used to plan where tissue samples should be taken for most accurate diagnosis during biopsy or surgical resection (129,141,151). This may be an important factor in distinguishing untreated grade III from grade II glioma, and targeting the highest CNI within the nonenhancing lesion is a sensible strategy (72). For patients with newly diagnosed grade IV glioma, higher levels of Lac and Lip in the region with abnormal CNI have been found to be associated with worse overall survival, even when controlling for the volume of CEL (74). This suggests that lesions that are both highly cellular and have regions of hypoxia and necrosis have a more malignant phenotype. This was found to be true for MRSI parameters obtained at both pre-surgical and pre-RT examinations (74,79).

The spatial extent of the metabolic lesion can also be used to plan focal therapy, such as external beam RT and gamma knife radiosurgery (36–38), and to assess the response to therapy. Figure 7 shows a patient with a grade IV glioma who had a relatively small residual

CEL prior to RT, but much more extensive T2L and metabolic lesions. At the post-RT and 2-month follow-up examinations, the surgical cavity became larger and there were changes in CEL that might have been mistaken for tumor progression. In both cases, the metabolic lesion, as defined by the number of shaded voxels with CNI greater than two, decreased. At the 4-month follow-up, there was continued resolution of the metabolic lesion and reduction in CEL.

Figure 8 shows the opposite example of a patient with a newly diagnosed grade IV glioma who had a gross total resection that showed an increase in T2L at the post-RT examination, but minimal change in CEL. By the 4-month follow-up, both T2L and CEL had become dramatically larger and the patient was designated as having tumor progression. It is clear from the MRSI data obtained at these time points that there is a substantial metabolic lesion at the pre-RT examination, which becomes larger at the post-RT examination and during follow-up. It should be noted that much of the area corresponding to CEL on the 4-month follow-up examination is necrotic, with the medial nonenhancing region having the highest Cho. These two examples show quite clearly that the information provided by MRSI data is complementary to the anatomic images, and may be more valuable than CEL in assessing treatment effects.

The differences in metabolite levels between gliomas with different histology can also be used to infer whether recurrent grade II gliomas have transformed to a higher grade. Figure 9 shows an example of a patient with an original diagnosis of grade II astrocytoma who was scanned immediately prior to surgery for suspected recurrence. The presence of diffuse enhancement on the T_1 post-gadolinium images, the moderate intensity on FLAIR and ADC images, and the increased rCBV in the lesion are suggestive of a more malignant phenotype. The metabolic signature of the lesion, as shown from the Lac-edited MRSI data, includes a large region with substantially increased Cho and reduced NAA, together with a central region that also shows Lip and Lac peaks. These are all characteristics of grade IV glioma. Histological analysis of tissue samples taken from regions with elevated CNI during image-guided surgery confirmed this diagnosis.

Another emerging MR metabolic imaging technology uses hyperpolarized ^{13}C agents to dramatically increase the sensitivity of the signal observed (159–161). The application of low temperatures and dynamic nuclear polarization, together with a rapid dissolution process, generates a sample that can be injected into living subjects. By providing a 10 000–50 000-fold signal enhancement, it is possible to observe the delivery and flux of endogenous, nontoxic and nonradioactive substances, such as pyruvate, through key biochemical pathways, such as glycolysis, the citric acid cycle and fatty acid synthesis (162). Preliminary studies have confirmed that ^{13}C-labeled pyruvate is delivered to tissues and converted to alanine, Lac and bicarbonate, with a spatial distribution and time course that varies according to the tissue of interest (163–165). This is of particular interest for the management of patients with glioma because the presence of Lac is a characteristic of high-grade glioma and is a prognostic factor for poor overall survival. Preliminary results in U-87 and U-251 tumors implanted into rat brain have shown that there is significantly higher ^{13}C-labeled Lac in tumor than in normal brain (166), and have demonstrated a reduction in the observed Lac within 1–2 days following treatment with temozolomide (167). This is likely to be critical for the identification of metabolically active Lac and hence for predicting whether a low-grade lesion has upgraded, and for assessing the response to therapy for patients with glioma.

CONCLUSIONS

Patients with glioma can benefit considerably from the integration of metabolic and physiological imaging into their conventional anatomic MRI examinations. Within a total scan time of 1 h, it is possible to obtain pre- and post-gadolinium T_1-weighted images, FLAIR or T_2-weighted images, diffusion tensor images, DCE and/or DSC images and MR metabolic images. The quantitative parameters derived from these data are valuable for predicting the tumor grade, directing tissue sampling during biopsy or surgical resection, defining the spatial extent of tumor for the planning of focal therapy and assessing the response to therapy. Table 1 shows the MR parameters that have been used in recent studies and have been shown to be relevant in evaluating the biological properties of the tumor. Further work is needed to standardize data acquisition and post-processing across institutions and scanners from different manufacturers, but there is no doubt that these techniques provide information that is important for making decisions concerning patient care. Combining such advanced MR methods into a single examination is especially critical for use in Phase I and Phase II clinical trials of combination therapies, which require multiple readouts to understand whether any of the treatments are having the anticipated effects and to identify biomarkers that can be used to tailor therapy to individual patient characteristics.

Acknowledgments

The author would like to thank Susan Chang and Soonmee Cha for helpful discussions concerning the topic of this review, as well as the staff, students and post-doctoral fellows at the Surbeck Laboratory at the University of California at San Francisco who participated in acquiring the data shown in the figures. This work was sponsored in part by National Institutes of Health (NIH) grants P50 CA 97257, PO1 CA118816 and RO1 CA127612.

Abbreviations used

ADC	apparent diffusion coefficient
BBB	blood–brain barrier
CEL	contrast-enhanced lesion
Cho	choline-containing compounds
CNI	choline to N-acetylaspartate index
Cre	creatine
DCE	dynamic contrast-enhanced
DSC	dynamic susceptibility-weighted contrast
DTI	diffusion tensor imaging
EV1, EV2, EV3	diffusion eigenvalues in three orthogonal directions
FA	fractional anisotropy
fBV	fractional blood volume
FDA	Food and Drug Administration
fDM	functional diffusion map
FLAIR	fluid-attenuated inversion recovery
GBM	glioblastoma multiforme
GPC	glycerophosphocholine

K_{trans}	fitted constant describing leakage of the contrast agent into the interstitial space
Lac	lactate
Lip	lipid
NAA	N-acetylaspartate
NAWM	normal-appearing white matter
nCBV	normalized cerebral blood volume
NEC	region of hypointensity on T1-weighted post-gadolinium images (necrosis)
PC	phosphocholine
PH	peak height of DSC curve
PRESS	point- resolved spectroscopy
RANO	Response Assessment in Neuro-Oncology
rCBV	relative cerebral blood volume
%REC	percentage recovery of the DSC signal to baseline
RECIST	Response Evaluation Criteria In Solid Tumors
RF	recirculation factor
ROI	region of interest
RT	radiation therapy
STEAM	stimulated echo acquisition mode
SWI	susceptibility-weighted imaging
T2L	T2 lesion
WHO	World Health Organization

References

1. Kleihues P, Burger PC, Scheithauer BW. The new WHO classification of brain tumours. Brain Pathol. 1993; 3:255–268. [PubMed: 8293185]
2. Daumas-Duport C, Tucker ML, Kolles H, Cervera P, Beuvon F, Varlet P, Udo N, Koziak M, Chodkiewicz JP. Oligodendrogliomas. Part II: A new grading system based on morphological and imaging criteria. J Neurooncol. 1997; 34:61–78. [PubMed: 9210053]
3. Louis DN, Ohgaki H, Wiestler OD, Cavenee WK, Burger PC, Jouvet A, Scheithauer BW, Kleihues P. The 2007 WHO classification of tumours of the central nervous system. Acta Neuropathol. 2007; 114:97–109. [PubMed: 17618441]
4. Brat DJ, Scheithauer BW, Fuller GN, Tihan T. Newly codified glial neoplasms of the 2007 WHO classification of tumours of the central nervous system: angiocentric glioma, pilomyxoid astrocytoma and pituicytoma. Brain Pathol. 2007; 17:319–324. [PubMed: 17598825]
5. Folkman J. The role of angiogenesis in tumor growth. Semin Cancer Biol. 1992; 3:65–71. [PubMed: 1378311]
6. Wesseling P, Ruiter DJ, Burger P. Angiogenesis in brain tumors: pathobiological and clinical aspects. J Neurooncol. 1997; 32:253–265. [PubMed: 9049887]
7. Sharma S, Sharma MC, Gupta DK, Sarkar C. Angiogenic patterns and their quantitation in high grade astrocytic tumors. J Neurooncol. 2006; 79:19–30. [PubMed: 16807783]

8. Schneider SW, Ludwig T, Tatenhorst L, Braune S, Oberleithner H, Senner V, Paulus W. Glioblastoma cells release factors that disrupt blood brain barrier features. Acta Neuropathol. 2004; 107:272–276. [PubMed: 14730455]

9. Ashby LS, Shapiro WR. Low-grade glioma: supratentorial astrocytoma, oligodendroglioma and oligoastrocytoma in adults. Curr Neurol Neurosci Rep. 2004; 4:211–217. [PubMed: 15102347]

10. Pignatti F, van den Bent M, Curran D, Debruyne C, Sylvester R, Therasse P, Afra D, Cornu P, Bolla M, Vecht C, Karim AB. European Organization for Research and Treatment of Cancer Brain Tumor Cooperative Group; European Organization for Research and Treatment of Cancer Radiotherapy Cooperative Group. Prognostic factors for survival in adult patients with cerebral low-grade glioma. J Clin Oncol. 2002; 20:2076–2084. [PubMed: 11956268]

11. Yeh SA, Ho JT, Lui CC, Huang YJ, Hsiung CY, Huang EY. Treatment outcomes and prognostic factors in patients with supratentorial low grade gliomas. Br J Radiol. 2005; 78:230–235. [PubMed: 15730987]

12. Lang F, Gilbert M. Diffusely infiltrative low grade gliomas in adults. J Clin Oncol. 2006; 24:1236–1245. [PubMed: 16525178]

13. Wallner KE, Galicich JH, Krol G, Arbit E, Malkin MG. Patterns of failure following treatment for glioblastoma multiforme and anaplastic astrocytoma. Int J Radiat Oncol Biol Phys. 1989; 16:1405–1409. [PubMed: 2542195]

14. Chan JL, Lee SW, Fraass BA, Normolle DP, Greenberg HS, Junck LR, Gebarski SS, Sandler HM. Survival and failure patterns of high-grade gliomas after three-dimensional conformal radiotherapy. J Clin Oncol. 2002; 20:1635–1642. [PubMed: 11896114]

15. Garden AS, Maor MH, Yung WK, Bruner JM, Woo SY, Moser RP, Lee YY. Outcome and patterns of failure following limited-volume irradiation for malignant astrocytomas. Radiother Oncol. 1991; 20:99–110. [PubMed: 1851573]

16. Liang BC, Thornton AF Jr, Sandler HM, Greenberg HS. Malignant astrocytomas: focal tumor recurrence after focal external beam radiation therapy. J Neurosurg. 1991; 75:559–563. [PubMed: 1653309]

17. Nakagawa K, Aoki Y, Fujimaki T, Tago M, Terahara A, Karasawa K, Sakata K, Sasaki Y, Matsutani M, Akanuma A. High-dose conformal radiotherapy influenced the pattern of failure but did not improve survival in glioblastoma multiforme. Int J Radiat Oncol Biol Phys. 1998; 40:1141–1149. [PubMed: 9539570]

18. Walker MD, Strike TA, Sheline GE. An analysis of dose–effect relationship in the radiotherapy of malignant gliomas. Int J Radiat Oncol Biol Phys. 1979; 5:1725–1731. [PubMed: 231022]

19. Bleehen NM, Stenning SP. A Medical Research Council trial of two radiotherapy doses in the treatment of grades 3 and 4 astrocytoma. The Medical Research Council Brain Tumour Working Party. Br J Cancer. 1991; 64:769–774. [PubMed: 1654987]

20. Sultanem K, Patrocinio H, Lambert C, Corns R, Leblanc R, Parker W, Shenouda G, Souhami L. The use of hypofractionated intensity-modulated irradiation in the treatment of glioblastoma multiforme: preliminary results of a prospective trial. Int J Radiat Oncol Biol Phys. 2004; 58:247–252. [PubMed: 14697445]

21. Floyd NS, Woo SY, Teh BS, Prado C, Mai WY, Trask T, Gildenberg PL, Holoye P, Augspurger ME, Carpenter LS, Lu HH, Chiu JK, Grant WH 3rd, Butler EB. Hypofractionated intensity-modulated radiotherapy for primary glioblastoma multiforme. Int J Radiat Oncol Biol Phys. 2004; 58:721–726. [PubMed: 14967426]

22. Souhami L, Seiferheld W, Brachman D, Podgorsak EB, Werner-Wasik M, Lustig R, Schultz CJ, Sause W, Okunieff P, Buckner J, Zamorano L, Mehta MP, Curran WJ Jr. Randomized comparison of stereotactic radiosurgery followed by conventional radiotherapy with carmustine to conventional radiotherapy with carmustine for patients with glioblastoma multiforme: report of Radiation Therapy Oncology Group 93-05 protocol. Int J Radiat Oncol Biol Phys. 2004; 60:853–860. [PubMed: 15465203]

23. Stupp R, Mason WP, van den Bent MJ, Weller M, Fisher B, Taphoorn MJ, Belanger K, Brandes AA, Marosi C, Bogdahn U, Curschmann J, Janzer RC, Ludwin SK, Gorlia T, Allgeier A, Lacombe D, Cairncross JG, Eisenhauer E, Mirimanoff RO. European Organisation for Research and Treatment of Cancer Brain Tumor and Radiotherapy Groups; National Cancer Institute of Canada

Clinical Trials Group. Radiotherapy plus concomitant and adjuvant temozolomide for glioblastoma. N Engl J Med. 2005; 352:987–996. [PubMed: 15758009]

24. Hegi ME, Diserens AC, Gorlia T, Hamou MF, de Tribolet N, Weller M, Kros JM, Hainfellner JA, Mason W, Mariani L, Bromberg JE, Hau P, Mirimanoff RO, Cairncross JG, Janzer RC, Stupp R. MGMT gene silencing and benefit from temozolomide in glioblastoma. N Engl J Med. 2005; 352:997–1003. [PubMed: 15758010]
25. Brada M, Viviers L, Abson C, Hines F, Britton J, Ashley S, Sardell S, Traish D, Gonsalves A, Wilkins P, Westbury C. Phase II study of primary temozolomide chemotherapy on patients with WHO grade II gliomas. Ann Oncol. 2003; 14:1715–1721. [PubMed: 14630674]
26. Hoang-Xuan K, Caplelle L, Kujas M, Taillibert S, Duffau H, Lejeune J, Polivka M, Crinière E, Marie Y, Mokhtari K, Carpentier AF, Laigle F, Simon JM, Cornu P, Broët P, Sanson M, Delattre JY. Temozolomide as initial treatment for adults with low grade oligodendrogliomas or oligoastrocytomas and correlation with chromosome 1p deletions. J Clin Oncol. 2004; 22:3133–3188. [PubMed: 15284265]
27. Quinn JA, Reardon DA, Freidman AH, Rich JN, Sampson JH, Provenzale JM, McLendon RE, Gururangan S, Bigner DD, Herndon JE 2nd, Avgeropoulos N, Finlay J, Tourt-Uhlig S, Affronti ML, Evans B, Stafford-Fox V, Zaknoen S, Friedman HS. Phase II trial of temozolomide in patients with progressive low grade glioma. J Clin Oncol. 2003; 21:646–651. [PubMed: 12586801]
28. Pace A, Vidiri A, Galie E, Carosi M, Telera S, Cianciulli AM, Canalini P, Giannarelli D, Jandolo B, Carapella CM. Temozolomide chemotherapy for progressive low grade glioma: clinical benefits and radiological response. Ann Oncol. 2003; 14:1722–1726. [PubMed: 14630675]
29. Buckner JC, Gesme D, O'Fallon JR, Hammack JE, Stafford S, Brown PD, Hawkins R, Scheithauer BW, Erickson BJ, Levitt R, Shaw EG, Jenkins R. Phase II trial of procarbazine, lomustine and vincristine as initial therapy for patients with low grade oligodendroglioma or oligoastrocytoma: efficacy and associations with chromosomal abnormalities. J Clin Oncol. 2003; 21:251–255. [PubMed: 12525516]
30. Stege EM, Kros JM, de Bruin HG, Enting RH, van Heuvel I, Looijenga LH, van der Rijt CD, Smitt PA, van den Bent MJ. Successful treatment of low grade oligodendroglial tumors with a chemotherapy regimen of procarbazinem, lomustine and vincristine. Cancer. 2005; 103:802–809. [PubMed: 15637687]
31. Sofietti R, Ruda R, Bradac G, Schiffer D. PCV chemotherapy for recurrent oligodendroglioma and oligoastrocytomas. Neurosurgery. 1998; 43:1066–1073. [PubMed: 9802850]
32. Hess KR, Wong ET, Jaeckle KA, Kyritsis AP, Levin VA, Prados MD, Yung WK. Response and progression in recurrent malignant glioma. Neuro-oncology. 1999; 1:282–288. [PubMed: 11550320]
33. Romanelli P, Conti A, Pontoriero A, Ricciardi GK, Tomasello F, De Renzis C, Innocenzi G, Esposito V, Cantore G. Role of stereotactic radiosurgery and fractionated stereotactic radiotherapy for the treatment of recurrent glioblastoma multiforme. Neurosurg Focus. 2009; 27:E8. Review. [PubMed: 19951061]
34. Yang I, Han S, Parsa AT. Heat-shock protein vaccines as active immunotherapy against human gliomas. Expert Rev Anticancer Ther. 2009; 9:1577–1582. [PubMed: 19895242]
35. Bobo RH, Laske DW, Akbasak A, Morrison PF, Dedrick RL, Oldfield EH. Convection-enhanced delivery of macromolecules in the brain. Proc Natl Acad Sci USA. 1994; 91:2076–2080. [PubMed: 8134351]
36. Lieberman DM, Laske DW, Morrison PF, Morrison PF, Dedrick RL, Oldfield EH. Convection-enhanced distribution of large molecules in gray matter during interstitial drug infusion. J Neurosurg. 1995; 82:1021–1029. [PubMed: 7539062]
37. Parney IF, Kunwar S, McDermott M, Berger M, Prados M, Cha S, Croteau D, Puri RK, Chang SM. Neuroradiographic changes following convection-enhanced delivery of the recombinant cytotoxin interleukin 13-PE38QQR for recurrent malignant glioma. J Neurosurg. 2005; 102:267–275. [PubMed: 15739554]
38. Brandsma D, Stalpers L, Taal W, Sminia P, van den Bent MJ. Clinical features, mechanisms, and management of pseudoprogression in malignant gliomas. Lancet Oncol. 2008; 9:453–461. [PubMed: 18452856]

39. Chamberlain MC, Glantz MJ, Chalmers L, Van Horn A, Sloan AE. Early necrosis following concurrent Temodar and radiotherapy in patients with glioblastoma. J Neurooncol. 2007; 82:81–83. [PubMed: 16944309]
40. Taal W, Brandsma D, de Bruin HG, Bromberg JE, Swaak-Kragten AT, Smitt PA, van Es CA, van den Bent MJ. Incidence of early pseudo-progression in a cohort of malignant glioma patients treated with chemoirradiation with temozolomide. Cancer. 2008; 113:405–410. [PubMed: 18484594]
41. Stupp R, Mason WP, van den Bent MJ, Weller M, Fisher B, Taphoorn MJ, Belanger K, Brandes AA, Marosi C, Bogdahn U, Curschmann J, Janzer RC, Ludwin SK, Gorlia T, Allgeier A, Lacombe D, Cairncross JG, Eisenhauer E, Mirimanoff RO. European Organisation for Research and Treatment of Cancer Brain Tumor and Radiotherapy Groups, National Cancer Institute of Canada Clinical Trials Group. Radiotherapy plus concomitant and adjuvant temozolomide for glioblastoma. N Engl J Med. 2005; 352:987–996. [PubMed: 15758009]
42. de Wit MC, de Bruin HG, Eijkenboom W, Sillevis Smitt PA, van den Bent MJ. Immediate post-radiotherapy changes in malignant glioma can mimic tumor progression. Neurology. 2004; 63:535–537. [PubMed: 15304589]
43. Chaskis C, Neyns B, Michotte A, De Ridder M, Everaert H. Pseudo-progression after radiotherapy with concurrent temozolomide for high-grade glioma: clinical observations and working recommendations. Surg Neurol. 2009; 72:423–428. [PubMed: 19150114]
44. Chamberlain MC, Glantz MJ, Chalmers L, Van Horn A, Sloan AE. Early necrosis following concurrent Temodar and radiotherapy in patients with glioblastoma. J Neurooncol. 2007; 82:81–83. [PubMed: 16944309]
45. Brandsma D, van den Bent MJ. Pseudoprogression and pseudore-sponse in the treatment of gliomas. Curr Opin Neurol. 2009; 22(6):633–638. [PubMed: 19770760]
46. Smith JS, Cha S, Mayo MC, McDermott MW, Parsa AT, Chang SM, Dillon WP, Berger MS. Serial diffusion-weighted magnetic resonance imaging in cases of glioma: distinguishing tumor recurrence from postresection injury. J Neurosurg. 2005; 103:428–438. [PubMed: 16235673]
47. Wong ET, Brem S. Taming glioblastoma: targeting angiogenesis. J Clin Oncol. 2007; 25(30): 4705–4706. [PubMed: 17947716]
48. Norden AD, Drappatz J, Muzikansky A, David K, Gerard M, McNamara MB, Phan P, Ross A, Kesari S, Wen PY. An exploratory survival analysis of anti-angiogenic therapy for recurrent malignant glioma. J Neurooncol. 2009; 92:149–155. [PubMed: 19043778]
49. Norden AD, Young GS, Setayesh K, Muzikansky A, Klufas R, Ross GL, Ciampa AS, Ebbeling LG, Levy B, Drappatz J, Kesari S, Wen PY. Bevacizumab for recurrent malignant gliomas: efficacy, toxicity, and patterns of recurrence. Neurology. 2008; 70:779–787. [PubMed: 18316689]
50. Narayana A, Kelly P, Golfinos J, Parker E, Johnson G, Knopp E, Zagzag D, Fischer I, Raza S, Medabalmi P, Eagan P, Gruber ML. Antiangiogenic therapy using bevacizumab in recurrent high-grade glioma: impact on local control and patient survival. J Neurosurg. 2009; 110:173–180. [PubMed: 18834263]
51. Norden AD, Drappatz J, Wen PY. Novel anti-angiogenic therapies for malignant gliomas. Lancet Neurol. 2008; 7:1152–1160. [PubMed: 19007739]
52. Rubenstein J, Kim J, Ozawa T, Zhang M, Westphal M, Deen DF, Shuman MA. Anti-VEGF antibody treatment of glioblastoma prolongs survival but results in increased vascular cooption. Neoplasia. 2000; 2:306–314. [PubMed: 11005565]
53. Paez-Ribes M, Allen E, Hudock J, Takeda T, Okuyama H, Viñals F, Inoue M, Bergers G, Hanahan D, Casanovas O. Antiangiogenic therapy elicits malignant progression of tumors to increased local invasion and distant metastasis. Cancer Cell. 2009; 15:220–231. [PubMed: 19249680]
54. Liu P, Cheng H, Roberts TM, Zhao JJ. Targeting the phosphoinositide 3-kinase pathway in cancer. Nat Rev Drug Discov. 2009; 8:627–644. [PubMed: 19644473]
55. Endersby R, Baker SJ. PTEN signaling in brain: neuropathology and tumorigenesis. Oncogene. 2008; 27:5416–5430. [PubMed: 18794877]
56. Chakravarti A, Palanichamy K. Overcoming therapeutic resistance in malignant gliomas: current practices and future directions. Cancer Treat Res. 2008; 139:173–18. [PubMed: 18236717]

57. Kelly WK, Richon VM, O'Connor O, Curley T, MacGregor-Curtelli B, Tong W, Klang M, Schwartz L, Richardson S, Rosa E, Drobnjak M, Cordon-Cordo C, Chiao JH, Rifkind R, Marks PA, Scher H. Phase I clinical trial of histone deacetylase inhibitor: suberoylanilide hydroxamic acid administered intravenously. Clin Cancer Res. 2003; 9:3578–3588. [PubMed: 14506144]
58. Isaacs JS, Xu W, Neckers L. Heat shock protein 90 as a molecular target for cancer therapeutics. Cancer Cell. 2003; 3:213–217. [PubMed: 12676580]
59. Cancer Genome Atlas Research Network. Comprehensive genomic characterization defines human glioblastoma genes and core pathways. Nature. 2008; 455:1061–1068. [PubMed: 18772890]
60. de Groot JF, Gilbert MR. New molecular targets in malignant gliomas. Curr Opin Neurol. 2007; 20:712–718. [PubMed: 17992095]
61. Macdonald D, Cascino T, Schold SJ, Cairncross JG. Response criteria for phase II studies of supratentorial malignant glioma. J Clin Oncol. 1990; 8:1277–1280. [PubMed: 2358840]
62. Van den Bent M, Volgelbaum M, Wen P, Macdonald DR, Chang SM. Endpoint assessment in gliomas: novel treatments limit the usefulness of the classical Macdonald criteria. J Clin Oncol. 2009; 27(18):2905–2908. [PubMed: 19451418]
63. Wen PY, Macdonald DR, Reardon DA, Cloughesy TF, Sorensen AG, Galanis E, Degroot J, Wick W, Gilbert MR, Lassman AB, Tsien C, Mikkelsen T, Wong ET, Chamberlain MC, Stupp R, Lamborn KR, Vogelbaum MA, van den Bent MJ, Chang SM. Updated response assessment criteria for high-grade gliomas: response assessment in neuro-oncology working group. J Clin Oncol. 2010; 28(11):1963–1972. [PubMed: 20231676]
64. Wedeen VJ, Hagmann P, Tseng WY, Reese TG, Weisskoff RM. Mapping complex tissue architecture with diffusion spectrum magnetic resonance imaging. Magn Reson Med. 2005; 54:1377–1386. [PubMed: 16247738]
65. Basser PJ, Pierpaoli C. Microstructural and physiological features of tissues elucidated by quantitative-diffusion-tensor MRI. J Magn Reson B. 1996; 111:209–219. [PubMed: 8661285]
66. Sugahara T, Korogi Y, Kochi M, Ikushima I, Shigematu Y, Hirai T, Okuda T, Liang L, Ge Y, Komohara Y, Ushio Y, Takahashi M. Usefulness of diffusion-weighted MRI with echoplanar technique in the evaluation of cellularity in gliomas. J Magn Reson Imaging. 1999; 9:53–60. [PubMed: 10030650]
67. Bello L, Castellano A, Fava E, Casaceli G, Riva M, Scotti G, Gaini SM, Falini A. Intraoperative use of diffusion tensor imaging fiber tractography and subcortical mapping for resection of gliomas: technical considerations. Neurosurg Focus. 2010; 28:E6. [PubMed: 20121441]
68. Berman JI, Berger MS, Chung SW, Nagarajan SS, Henry RG. Accuracy of diffusion tensor magnetic resonance imaging tractography assessed using intraoperative subcortical stimulation mapping and magnetic source imaging. J Neurosurg. 2007; 107:488–494. [PubMed: 17886545]
69. Bian W, Khayal IS, Lupo JM, McGue C, Vandenberg S, Lamborn KR, Chang SM, Cha S, Nelson SJ. Multiparametric characterization of grade 2 glioma subtypes using magnetic resonance spectroscopic, perfusion, and diffusion imaging. Transl Oncol. 2009; 2:271–280. [PubMed: 19956389]
70. Khayal IS, Nelson SJ. Characterization of low-grade gliomas using RGB color maps derived from ADC histograms. J Magn Reson Imaging. 2009; 30:209–213. [PubMed: 19557741]
71. Khayal IS, McKnight TR, McGue C, Vandenberg S, Lamborn KR, Chang SM, Cha S, Nelson SJ. Apparent diffusion coefficient and fractional anisotropy of newly diagnosed grade II gliomas. NMR Biomed. 2009; 22:449–455. [PubMed: 19125391]
72. Chang SM, Nelson S, Vandenberg S, Cha S, Prados M, Butowski N, McDermott M, Parsa AT, Aghi M, Clarke J, Berger M. Integration of preoperative anatomic and metabolic physiologic imaging of newly diagnosed glioma. J Neurooncol. 2009; 92:401–415. [PubMed: 19357966]
73. Padhani AR, Liu G, Mu-Koh D, Chenevert TL, Thoeny HC, Takahara T, Dzik-Jurasz A, Ross BD, Van Cauteren M, Collins D, Hammoud DA, Rustin GJ, Taouli B, Choyke PL. Diffusion-weighted magnetic resonance imaging as a cancer biomarker: consensus and recommendations. Neoplasia. 2009; 11:102–125. [PubMed: 19186405]
74. Crawford FW, Khayal IS, McGue C, Saraswathy S, Pirzkall A, Cha S, Lamborn KR, Chang SM, Berger MS, Nelson SJ. Relationship of pre-surgery metabolic and physiological MR imaging

parameters to survival for patients with untreated GBM. J Neurooncol. 2009; 91(3):337–351. [PubMed: 19009235]

75. Yamasaki F, Kurisu K, Satoh K, Arita K, Sugiyama K, Ohtaki M, Takaba J, Tominaga A, Hanaya R, Yoshioka H, Hama S, Ito Y, Kajiwara Y, Yahara K, Saito T, Thohar MA. Apparent diffusion coefficient of human brain tumors at MR imaging. Radiology. 2005; 235:985–991. [PubMed: 15833979]
76. Lam WWM, Poon WS, Metreweil C. Diffusion MR imaging in glioma: does it have any role in the pre-operation determination of grading of glioma? Clin. Radiol. 2002; 57:219–225.
77. Inoue T, Ogasawara K, Beppu T, Ogawa A, Kabasawa H. Diffusion tensor imaging for preoperative evaluation of tumor grade in gliomas. Clin Neurol Neurosurg. 2005; 107:174–180. [PubMed: 15823671]
78. Pirzkall A, McGue C, Saraswathy S, Cha S, Liu R, Vandenberg S, Lamborn KR, Berger MS, Chang SM, Nelson SJ. Tumor regrowth between surgery and initiation of adjuvant therapy in patients with newly diagnosed glioblastoma. Neuro-oncology. 2009; 11:842–852. [PubMed: 19229057]
79. Saraswathy S, Crawford FW, Lamborn KR, Pirzkall A, Chang S, Cha S, Nelson SJ. Evaluation of MR markers that predict survival in patients with newly diagnosed GBM prior to adjuvant therapy. J Neurooncol. 2009; 91:69–81. [PubMed: 18810326]
80. Oztürk A, Oğuz KK, Akalan N, Geyik PO, Cila A. Evaluation of parenchymal changes at the operation site with early postoperative brain diffusion-weighted magnetic resonance imaging. Diagn Interv Radiol. 2006; 12:115–120. [PubMed: 16972214]
81. Chenevert TL, Stegman LD, Taylor JM, Robertson PL, Greenberg HS, Rehemtulla A, Ross BD. Diffusion magnetic resonance imaging: an early surrogate marker of therapeutic efficacy in brain tumors. J Natl Cancer Inst. 2000; 92:2029–2036. [PubMed: 11121466]
82. Mardor Y, Roth Y, Lidar Z, Jonas T, Pfeffer R, Maier SE, Faibel M, Nass D, Hadani M, Orenstein A, Cohen JS, Ram Z. Monitoring response to convection-enhanced taxol delivery in brain tumor patients using diffusion-weighted magnetic resonance imaging. Cancer Res. 2001; 61:4971–4973. [PubMed: 11431326]
83. Mardor Y, Pfeffer R, Spiegelmann R, Roth Y, Maier SE, Nissim O, Berger R, Glicksman A, Baram J, Orenstein A, Cohen JS, Tichler T. Early detection of response to radiation therapy in patients with brain malignancies using conventional and high b-value diffusion-weighted magnetic resonance imaging. J Clin Oncol. 2003; 21:1094–1100. [PubMed: 12637476]
84. Moffat BA, Chenevert TL, Lawrence TS, Meyer CR, Johnson TD, Dong Q, Tsien C, Mukherji S, Quint DJ, Gebarski SS, Robertson PL, Junck LR, Rehemtulla A, Ross BD. Functional diffusion map: a noninvasive MRI biomarker for early stratification of clinical brain tumor response. Proc Natl Acad Sci USA. 2005; 102:5524–5529. [PubMed: 15805192]
85. Hamstra DA, Chenevert TL, Moffat BA, Johnson TD, Meyer CR, Mukherji SK, Quint DJ, Gebarski SS, Fan X, Tsien CI, Lawrence TS, Junck L, Rehemtulla A, Ross BD. Evaluation of the functional diffusion map as an early biomarker of time-to-progression and overall survival in high-grade glioma. Proc Natl Acad Sci USA. 2005; 102:16759–16764. [PubMed: 16267128]
86. Moffat BA, Chenevert TL, Meyer CR, McKeever PE, Hall DE, Hoff BA, Johnson TD, Rehemtulla A, Ross BD. The functional diffusion map: an imaging biomarker for the early prediction of cancer treatment outcome. Neoplasia. 2006; 8:259–267. [PubMed: 16756718]
87. Hamstra DA, Rehemtulla A, Ross BD. Diffusion magnetic resonance imaging: a biomarker for treatment response in oncology. J Clin Oncol. 2007; 25:4104–4109. [PubMed: 17827460]
88. Hamstra DA, Galban CJ, Meyer CR, Johnson TD, Sundgren PC, Tsien C, Lawrence TS, Junck L, Ross DJ, Rehemtulla A, Ross BD, Chenevert TL. Functional diffusion map as an early imaging biomarker for high-grade glioma: correlation with conventional radiologic response and overall survival. J Clin Oncol. 2008; 26:3387–3394. [PubMed: 18541899]
89. Minamikawa S, Kono K, Nakayama K, Yokote H, Tashiro T, Nishio A, Hara M, Inoue Y. Glucocorticoid treatment of brain tumor patients: changes of apparent diffusion coefficient values measured by MR diffusion imaging. Neuroradiology. 2004; 46:805–811. [PubMed: 15448954]

90. Khayal IS, Polley MY, Jalbert L, Elkhaled A, Chang SM, Cha S, Butowski NA, Nelson SJ. Evaluation of diffusion parameters as early biomarkers of disease progression in glioblastoma multiforme. Neuro-oncology. 2010; 12:908–916. [PubMed: 20501631]

91. Pope WB, Kim HJ, Huo J, Alger J, Brown MS, Gjertson D, Sai V, Young JR, Tekchandani L, Cloughesy T, Mischel PS, Lai A, Nghiemphu P, Rahmanuddin S, Goldin J. Recurrent glioblastoma multiforme: ADC histogram analysis predicts response to bevacizumab treatment. Radiology. 2009; 252:182–189. [PubMed: 19561256]

92. Li Y, Lupo JM, Polley M, Crane JC, Bian W, Cha S, Chang SM, Nelson SJ. Serial analysis of imaging parameters in patients with newly diagnosed glioblastoma multiforme. Neuro-oncology. 201110.1093/neuonc/noq194

93. Tozer DJ, Jäger HR, Danchaivijitr N, Benton CE, Tofts PS, Rees JH, Waldman AD. Apparent diffusion coefficient histograms may predict low-grade glioma subtype. NMR Biomed. 2007; 20:49–57. [PubMed: 16986106]

94. Elkhaled, A.; Jalbert, L.; Yoshihara, H.; Bourne, G.; Cloyd, C.; Phillips, J.; Cha, S.; Chang, SM.; Kurhanewicz, J.; Srinivasan, R.; Nelson, SJ. Comparison of glioma sub-populations using in-vivo ADC values and ex-vivo ^{1}H HR-MAS spectroscopy. Proceedings of the 18th Annual Meeting ISMRM; Stockholm: Sweden. 2010. p. 2203

95. Rosen BR, Belliveau JW, Chien D. Perfusion imaging by nuclear magnetic resonance. Magn Reson Q. 1989; 5:263–281. [PubMed: 2701285]

96. Edelman RR, Mattle HP, Atkinson DJ, Hill T, Finn JP, Mayman C, Ronthal M, Hoogewoud HM, Kleefield J. Cerebral blood flow: assessment with dynamic contrast-enhanced T2*-weighted MR imaging at 1. 5 T. Radiology. 1990; 176:211–220. [PubMed: 2353094]

97. Aronen HJ, Gazit IE, Louis DN, Buchbinder BR, Pardo FS, Weisskoff RM, Harsh GR, Cosgrove GR, Halpern EF, Hochberg FH. Cerebral blood volume maps of gliomas: comparison with tumor grade and histologic findings. Radiology. 1994; 191:41–51. [PubMed: 8134596]

98. Guckel F, Brix G, Rempp K, Deimling M, Rother J, Georgi M. Assessment of cerebral blood volume with dynamic susceptibility contrast enhanced gradient-echo imaging. J Comput Assist Tomogr. 1994; 18:344–351. [PubMed: 8188897]

99. Knopp EA, Cha S, Johnson G, Mazumdar A, Golfinos JG, Zagzag D, Miller DC, Kelly PJ, Kricheff II. Glial neoplasms: dynamic contrast-enhanced T2*-weighted MR imaging. Radiology. 1999; 211:791–798. [PubMed: 10352608]

100. Sugahara T, Korogi Y, Kochi M, Ikushima I, Hirai T, Okuda T, Shigematsu Y, Liang L, Ge Y, Ushio Y, Takahashi M. Correlation of MR imaging-determined cerebral blood volume maps with histologic and angiographic determination of vascularity of gliomas. Am J Roentgenol. 1998; 171:1479–1486. [PubMed: 9843274]

101. Lee MC, Chang SM, Cha S, Nelson SJ. Dynamic susceptibility contrast perfusion imaging of radiation effects in normal appearing brain tissue: changes in the first-pass and recirculation phases. J Magn Reson Imaging. 2005; 21:683–693. [PubMed: 15906330]

102. Lupo JM, Cha S, Sadarangani P, Chang S, Nelson SJ. Dynamic susceptibility-weighted perfusion imaging of high-grade gliomas: characterization of spatial heterogeneity. Am J Neuroradiol. 2005; 26:1446–1454. [PubMed: 15956514]

103. Lupo JM, Cha S, Chang SM, Nelson SJ. Analysis of metabolic indices in regions of abnormal perfusion in patients with high-grade glioma. Am J Neuroradiol. 2007; 28:1455–1461. [PubMed: 17846190]

104. Lacerda S, Law M. Magnetic resonance perfusion and permeability imaging in brain tumors. Neuroimaging Clin N Am. 2009; 19:527–557. [PubMed: 19959004]

105. Mills SJ, Soh C, O'Connor JP, Rose CJ, Buonaccorsi G, Cheung S, Zhao S, Parker GJ, Jackson A. Enhancing fraction in glioma and its relationship to the tumoral vascular microenvironment: a dynamic contrast-enhanced MR imaging study. Am J Neuroradiol. 2010; 31:726–731. [PubMed: 20019100]

106. Barboriak DP, MacFall JR, Viglianti BL, Dewhirst Dvm MW. Comparison of three physiologically-based pharmacokinetic models for the prediction of contrast agent distribution measured by dynamic MR imaging. J Magn Reson Imaging. 2008; 27:1388–1398. [PubMed: 18504759]

107. Evelhoch J, Garwood M, Vigneron D, Knopp M, Sullivan D, Menkens A, Clarke L, Liu G. Expanding the use of magnetic resonance in the assessment of tumor response to therapy: workshop report. Cancer Res. 2005; 65:7041–7044. [PubMed: 16103049]

108. Ashton E, Raunig D, Ng C, Kelcz F, McShane T, Evelhoch J. Scan–rescan variability in perfusion assessment of tumors in MRI using both model and data-derived arterial input functions. J Magn Reson Imaging. 2008; 28:791–796. [PubMed: 18777526]

109. Ferl GZ, Xu L, Friesenhahn M, Bernstein LJ, Barboriak DP, Port RE. An automated method for nonparametric kinetic analysis of clinical DCE-MRI data: application to glioblastoma treated with bevacizumab. Magn Reson Med. 2010; 63:1366–1375. [PubMed: 20432307]

110. Harrer JU, Parker GJ, Haroon HA, Buckley DL, Embelton K, Roberts C, Balriaux D, Jackson A. Comparative study of methods for determining vascular permeability and blood volume in human gliomas. J Magn Reson Imaging. 2004; 20(5):748–757. [PubMed: 15503330]

111. Tofts PS, Kermode AG. Measurement of the blood–brain barrier permeability and leakage space using dynamic MR imaging. 1. Fundamental concepts. Magn Reson Med. 1991; 17:357–367. [PubMed: 2062210]

112. Hu LS, Baxter LC, Pinnaduwage DS, Paine TL, Karis JP, Feuerstein BG, Schmainda KM, Dueck AC, Debbins J, Smith KA, Nakaji P, Eschbacher JM, Coons SW, Heiserman JE. Optimized preload leakage-correction methods to improve the diagnostic accuracy of dynamic susceptibility-weighted contrast-enhanced perfusion MR imaging in post-treatment gliomas. Am J Neuroradiol. 2010; 31:40–48. [PubMed: 19749223]

113. Hu LS, Baxter LC, Smith KA, Feuerstein BG, Karis JP, Eschbacher JM, Coons SW, Nakaji P, Yeh RF, Debbins J, Heiserman JE. Relative cerebral blood volume values to differentiate high-grade glioma recurrence from posttreatment radiation effect: direct correlation between image-guided tissue histopathology and localized dynamic susceptibility-weighted contrast-enhanced perfusion MR imaging measurements. Am J Neuroradiol. 2009; 30:552–558. [PubMed: 19056837]

114. Paulson ES, Schmainda KM. Comparison of dynamic susceptibility-weighted contrast-enhanced MR methods: recommendations for measuring relative cerebral blood volume in brain tumors. Radiology. 2008; 249:601–613. [PubMed: 18780827]

115. Boxerman JL, Schmainda KM, Weisskoff RM. Relative cerebral blood volume maps corrected for contrast agent extravasation significantly correlate with glioma tumor grade, whereas uncorrected maps do not. Am J Neuroradiol. 2006; 27:859–867. [PubMed: 16611779]

116. Law M, Yang S, Wang H, Babb JS, Johnson G, Cha S, Knopp EA, Zagzag D. Glioma grading: sensitivity, specificity, and predictive values of perfusion MR imaging and proton MR spectroscopic imaging compared with conventional MR imaging. Am J Neuroradiol. 2003; 24:1989–1998. [PubMed: 14625221]

117. Catalaa I, Henry R, Dillon WP, Graves EE, McKnight TR, Lu Y, Vigneron DB, Nelson SJ. Perfusion, diffusion and spectroscopy values in newly diagnosed cerebral gliomas. NMR Biomed. 2006; 19:463–475. [PubMed: 16763973]

118. Cha S, Tihan T, Crawford F, Fischbein NJ, Chang S, Bollen A, Nelson SJ, Prados M, Berger MS, Dillon WP. Differentiation of low-grade oligodendrogliomas from low-grade astrocytomas using quantitative blood-volume measurements derived from dynamic susceptibility contrast-enhanced MR imaging. Am J Neuroradiol. 2005; 26:266–273. [PubMed: 15709123]

119. Batchelor TT, Sorensen AG, di Tomaso E, Zhang WT, Duda DG, Cohen KS, Kozak KR, Cahill DP, Chen PJ, Zhu M, Ancukiewicz M, Mrugala MM, Plotkin S, Drappatz J, Louis DN, Ivy P, Scadden DT, Benner T, Loeffler JS, Wen PY, Jain RK. AZD2171, a pan-VEGF receptor tyrosine kinase inhibitor, normalizes tumor vasculature and alleviates edema in glioblastoma patients. Cancer Cell. 2007; 11:83–95. [PubMed: 17222792]

120. Barajas RF Jr, Chang JS, Segal MR, Parsa AT, McDermott MW, Berger MS, Cha S. Differentiation of recurrent glioblastoma multiforme from radiation necrosis after external beam radiation therapy with dynamic susceptibility-weighted contrast-enhanced perfusion MR imaging. Radiology. 2009; 253:486–496. [PubMed: 19789240]

121. Essock-Burn E, Lupo JM, Cha S, Polley M, Butowski NA, Chang SM, Nelson SJ. Assessment of perfusion MRI derived parameters in evaluating and predicting response to anti-angiogenic

therapy in patients with newly diagnosed GBM. Neuro-oncology. 2011; 13(1):119–131. [PubMed: 21036812]

122. Lupo JM, Banerjee S, Hammond KE, Kelley DA, Xu D, Chang SM, Vigneron DB, Majumdar S, Nelson SJ. GRAPPA-based susceptibility-weighted imaging of normal volunteers and patients with brain tumor at 7 T. Magn Reson Imaging. 2009; 27:480–488. [PubMed: 18823730]
123. Lupo, JM.; Chuang, C.; Jimenez, B.; Chang, SM.; Barani, IJ.; Hess, CP.; Nelson, SJ. Assessing the effects of radiation therapy on normal brain tissue in patients with glioma using susceptibility-weighted imaging at 7 Tesla. Proc Intl Soc Mag Reson Med; Proceedings of the 18th Annual Meeting ISMRM; Stockholm: Sweden. 2010; 2010.
124. Luyten PR, Marien AJ, Heindel W, van Gerwen PH, Herholz K, den Hollander JA, Friedmann G, Heiss WD. Metabolic imaging of patients with intracranial tumors: H-1 MR spectroscopic imaging and PET. Radiology. 1990; 176:791–799. [PubMed: 2389038]
125. Demaerel P, Johannik K, Van Hecke P, Van Ongeval C, Verellen S, Marchal G, Wilms G, Plets C, Goffin J, Van Calenbergh F. Localized ^{1}H NMR spectroscopy in fifty cases of newly diagnosed intracranial tumors. J. Comput. Assist. Tomogr. 1991; 15:67–76.
126. Usenius JP, Kauppinen RA, Vainio PA, Hernesniemi JA, Vapalahti MP, Paljarvi LA, Soimakallio S. Quantitative metabolite patterns of human brain tumors: detection by ^{1}H NMR spectroscopy in vivo and in vitro. J. Comput. Assist. Tomogr. 1994; 18:705–713.
127. Fulham MJ, Bizzi A, Dietz MJ, Shih HH, Raman R, Sobering GS, Frank JA, Dwyer AJ, Alger JR, Di Chiro G. Mapping of brain tumor metabolites with proton MR spectroscopic imaging: clinical relevance. Radiology. 1992; 185:675–686. [PubMed: 1438744]
128. Negendank WG, Sauter R, Brown TR, Evelhoch JL, Falini A, Gotsis ED, Heerschap A, Kamada K, Lee BC, Mengeot MM, Moser E, Padavic-Shaller KA, Sanders JA, Spraggins TA, Stillman AE, Terwey B, Vogl TJ, Wicklow K, Zimmerman RA. Proton magnetic resonance spectroscopy in patients with glial tumors: a multicenter study. J Neurosurg. 1996; 84:449–458. [PubMed: 8609557]
129. Preul MC, Caramanos Z, Collins DL, Villemure JG, Leblanc R, Olivier A, Pokrupa R, Arnold DL. Accurate, noninvasive diagnosis of human brain tumors by using proton magnetic resonance spectroscopy. Nat Med. 1996; 2:323–325. [PubMed: 8612232]
130. Go KG, Kammam RL, Mooyaart EL, Heesters MA, Pruim J, Vaalburg W, Paans AM. Localised proton spectroscopy and spectroscopic imaging in cerebral gliomas, with comparison to positron emission tomography. Neuroradiology. 1995; 37(3):198–206. [PubMed: 7603595]
131. Dowling C, Bollen AW, Noworolski SM, McDermott MW, Barbaro NM, Day MR, Henry RG, Chang SM, Dillon WP, Nelson SJ, Vigneron DB. Preoperative proton MR spectroscopic imaging of brain tumors: correlation with histopathologic analysis of resection specimens. Am J Neuroradiol. 2001; 22:604–612. [PubMed: 11290466]
132. Nelson SJ, Vigneron DB, Dillon WP. Serial evaluation of patients with brain tumors using volume MRI and 3D ^{1}H MRSI. NMR Biomed. 1999; 12(3):123–138. [PubMed: 10414947]
133. Heesters MA, Kamman RL, Mooyaart EL, Go KG. Localized proton spectroscopy of inoperable brain gliomas. Response to radiation therapy. J Neurooncol. 1993; 17:27–35. [PubMed: 8120569]
134. Li Y, Osorio JA, Ozturk-Isik E, Chen AP, Xu D, Crane JC, Cha S, Chang S, Berger MS, Vigneron DB, Nelson SJ. Considerations in applying 3D PRESS H-1 brain MRSI with an eight-channel phased-array coil at 3 T. Magn Reson Imaging. 2006; 24:1295–1302. [PubMed: 17145400]
135. Osorio JA, Ozturk-Isik E, Xu D, Cha S, Chang S, Berger MS, Vigneron DB, Nelson SJ. 3D MRSI of brain tumors at 3 Tesla using an 8 channel phased array head coil. J Magn Reson Imaging. 2007; 26:23–30. [PubMed: 17659562]
136. Zierhut ML, Ozturk-Isik E, Chen AP, Park I, Vigneron DB, Nelson SJ. (1)H spectroscopic imaging of human brain at 3 Tesla: comparison of fast three-dimensional magnetic resonance spectroscopic imaging techniques. J Magn Reson Imaging. 2009; 30:473–480. [PubMed: 19711396]

137. Ozturk-Isik E, Crane JC, Cha S, Chang SM, Berger MS, Nelson SJ. Unaliasing lipid contamination for MR spectroscopic imaging of gliomas at 3T using sensitivity encoding (SENSE). Magn Reson Med. 2006; 55:1164–1169. [PubMed: 16596629]

138. Ozturk E, Banerjee S, Majumdar S, Nelson SJ. Partially parallel MR spectroscopic imaging of gliomas at3T. Conf Proc IEEE Eng Med Biol Soc. 2006; 1:493–496. [PubMed: 17945589]

139. Cheng LL, Ma MJ, Becerra L, Ptak T, Tracey I, Lackner A, González RG. Quantitative neuropathology by high resolution magic angle spinning proton magnetic resonance spectroscopy. Proc Natl Acad Sci USA. 1997; 94:6408–6413. [PubMed: 9177231]

140. Cheng LL, Chang IW, Louis DN, Gonzalez RG. Correlation of high-resolution magic angle spinning proton magnetic resonance spectroscopy with histopathology of intact human brain tumor specimens. Cancer Res. 1998; 58:1825–1832. [PubMed: 9581820]

141. Barbarella G, Ricci R, Pirini G, Tugnoli V, Tosi MR, Bertoluzza A, Calbucci F, Leonardi M, Trevisan C, Eusebi V. In vivo single voxel ^{1}H MRS of glial brain tumors: correlation with tissue histology and in vitro MRS. Int J Oncol. 1998; 12:461–468. [PubMed: 9458376]

142. McKnight TR, von dem Bussche MH, Vigneron DB, Lu Y, Berger MS, McDermott MW, Dillon WP, Graves EE, Pirzkall A, Nelson S. Histopathological validation of a three-dimensional magnetic resonance spectroscopy index as a predictor of tumor presence. J Neurosurg. 2002; 97:794–802. [PubMed: 12405365]

143. Pirzkall A, McKnight TR, Graves EE, Carol MP, Sneed PK, Wara WW, Nelson SJ, Verhey LJ, Larson DA. MR-spectroscopy guided target delineation for high-grade gliomas. Int J Radiat Oncol Biol Phys. 2001; 50:915–928. [PubMed: 11429219]

144. Pirzkall A, Li X, Oh J, Chang S, Berger MS, Larson DA, Verhey LJ, Dillon WP, Nelson SJ. 3D MRSI for resected high-grade gliomas before RT: tumor extent according to metabolic activity in relation to MRI. Int J Radiat Oncol Biol Phys. 2004; 59:126–137. [PubMed: 15093908]

145. Graves EE, Nelson SJ, Vigneron DB, Chin C, Verhey L, McDermott M, Larson D, Sneed PK, Chang S, Prados MD, Lamborn K, Dillon WP. A preliminary study of the prognostic value of proton magnetic resonance spectroscopic imaging in gamma knife radiosurgery of recurrent malignant gliomas. Neurosurgery. 2000; 46:319–326. [PubMed: 10690720]

146. Graves EE, Nelson SJ, Vigneron DB, Verhey L, McDermott M, Larson D, Chang S, Prados MD, Dillon WP. Serial proton MR spectroscopic imaging of recurrent malignant gliomas after gamma knife radiosurgery. Am J Neuroradiol. 2001; 22:613–624. [PubMed: 11290467]

147. Chan AA, Lau A, Pirzkall A, Chang SM, Verhey LJ, Larson D, McDermott MW, Dillon WP, Nelson SJ. Proton magnetic resonance spectroscopy imaging in the evaluation of patients undergoing gamma knife surgery for Grade IV glioma. J Neurosurg. 2004; 101:467–475. [PubMed: 15352605]

148. Nelson SJ, Graves E, Pirzkall A, Li X, Antiniw Chan A, Vigneron DB, McKnight TR. In vivo molecular imaging for planning radiation therapy of gliomas: an application of ^{1}H MRSI. J. Magn. Reson Imaging. 2002; 16:464–476.

149. Park I, Tamai G, Lee MC, Chuang CF, Chang SM, Berger MS, Nelson SJ, Pirzkall A. Patterns of recurrence analysis in newly diagnosed glioblastoma multiforme after three-dimensional conformal radiation therapy with respect to pre-radiation therapy magnetic resonance spectroscopic findings. Int J Radiat Oncol Biol Phys. 2007; 69:381–389. [PubMed: 17513061]

150. Rock JP, Hearshen D, Scarpace L, Croteau D, Gutierrez J, Fisher JL, Rosenblum ML, Mikkelsen T. Correlations between magnetic resonance spectroscopy and image-guided histopathology, with special attention to radiation necrosis. Neurosurgery. 2002; 51:912–919. [PubMed: 12234397]

151. McKnight TR, Noworolski SM, Vigneron DB, Nelson SJ. An automated technique for the quantitative assessment of 3D-MRSI data from patients with glioma. J Magn Reson Imaging. 2001; 13:167–177. [PubMed: 11169821]

152. Lee MC, Pirzkall A, McKnight TR, Nelson SJ. 1H-MRSI of radiation effects in normal-appearing white matter: dose-dependence and impact on automated spectral classification. J Magn Reson Imaging. 2004; 19:379–388. [PubMed: 15065160]

153. Matulewicz L, Sokol M, Michnik A, Wydmanski J. Long-term normal-appearing brain tissue monitoring after irradiation using proton magnetic resonance spectroscopy in vivo: statistical

analysis of a large group of patients. Int J Radiat Oncol Biol Phys. 2006; 66:825–832. [PubMed: 16949766]

154. Esteve F, Rubin C, Grand S, Kolodie H, Le Bas JF. Transient metabolic changes observed with proton MR spectroscopy in normal human brain after radiation therapy. Int J Radiat Oncol Biol Phys. 1998; 40:279–286. [PubMed: 9457810]
155. Park I, Chen AP, Zierhut ML, Ozturk-Isik E, Vigneron DB, Nelson SJ. Implementation of 3 T lactate-edited 3D (1)H MR spectroscopic imaging with flyback echoplanar readout for gliomas patients. Ann Biomed Eng. 2011; 39(1):193–204. [PubMed: 20652745]
156. Wright AJ, Fellows G, Byrnes TJ, Opstad KS, McIntyre DJ, Griffiths JR, Bell BA, Clark CA, Barrick TR, Howe FA. Pattern recognition of MRSI data shows regions of glioma growth that agree with DTI markers of brain tumor infiltration. Magn Reson Med. 2009; 62:1646–1651. [PubMed: 19785020]
157. Opstad KS, Wright AJ, Bell BA, Griffiths JR, Howe FA. Correlations between in vivo (1)H MRS and ex vivo (1)H HRMAS metabolite measurements in adult human gliomas. J Magn Reson Imaging. 2010; 31:289–297. [PubMed: 20099340]
158. Srinivasan R, Phillips JJ, Vandenberg SR, Polley MY, Bourne G, Au A, Pirzkall A, Cha S, Chang SM, Nelson SJ. Ex vivo MR spectroscopic measure differentiates tumor from treatment effects in GBM. Neuro Oncol. 2010; 12(11):1152–1161. [PubMed: 20647244]
159. Ardenkjaer-Larsen JH, Fridlund B, Gram A, Hansson G, Hansson L, Lerche MH, Servin R, Thaning M, Golman K. Increase in signal-to-noise ratio of > 10,000 times in liquid-state NMR. Proc Natl Acad Sci USA. 2003; 100(10):158.
160. Golman K, Zandt R, Thaning M. Real-time metabolic imaging. Proc Natl Acad Sci USA. 2006; 103(30):11270–11275. [PubMed: 16837573]
161. Golman K, Zandt RI, Lerche M, Pehrson R, Ardenkjaer-Larsen JH. Metabolic imaging by hyperpolarized ^{13}C magnetic resonance imaging for in vivo tumor diagnosis. Cancer Res. 2006; 66:10855–10860. [PubMed: 17108122]
162. Nelson SJ, Vigneron D, Kurhanewicz J, Chen A, Bok R, Hurd R. DNP-hyperpolarized ^{13}C magnetic resonance metabolic imaging for cancer applications. Appl. Magn. Reson. 2008; 34:533–544.
163. Kohler SJ, Yen Y, Wolber J, Chen AP, Albers MJ, Bok R, Zhang V, Tropp J, Nelson SJ, Vigneron DB, Kurhanewicz J, Hurd RE. In vivo ^{13}Carbon metabolic imaging at 3T with hyperpolarized ^{13}C-1-pyruvate. Magn Reson Med. 2007; 58(1):65–69. [PubMed: 17659629]
164. Chen AP, Albers MJ, Cunningham CH, Kohler SJ, Yen YF, Hurd RE, Tropp J, Bok R, Pauly JM, Nelson SJ, Kurhanewicz J, Vigneron DB. Hyperpolarized ^{13}C spectroscopic imaging of the TRAMP mouse at 3T – initial experience. Magn Reson Med. 2007; 58:1099–1106. [PubMed: 17969006]
165. Albers MJ, Bok R, Chen AP, Cunningham CH, Zierhut ML, Zhang VY, Kohler SJ, Tropp J, Hurd RE, Yen YF, Nelson SJ, Vigneron DB, Kurhanewicz J. Hyperpolarized ^{13}C lactate, pyruvate, and alanine: noninvasive biomarkers for prostate cancer detection and grading. Cancer Res. 2008; 68:8607–8615. [PubMed: 18922937]
166. Park I, Larson PE, Zierhut ML, Hu S, Bok R, Ozawa T, Kurhanewicz J, Vigneron DB, Vandenberg SR, James CD, Nelson SJ. Hyperpolarized ^{13}C magnetic resonance metabolic imaging: application to brain tumors. Neuro-oncology. 2010; 12:133–144. [PubMed: 20150380]
167. Park, I.; Chaumeil, M.; Ozawa, T.; Ronen, SM.; Vigneron, DB.; James, C.; Nelson, SJ. Detection of early response to temozolomide treatment in brain tumors using hyperpolarized ^{13}C MR metabolic imaging. Proceedings of the 18th Annual Meeting ISMRM; Stockholm: Sweden. 2010. p. 3732

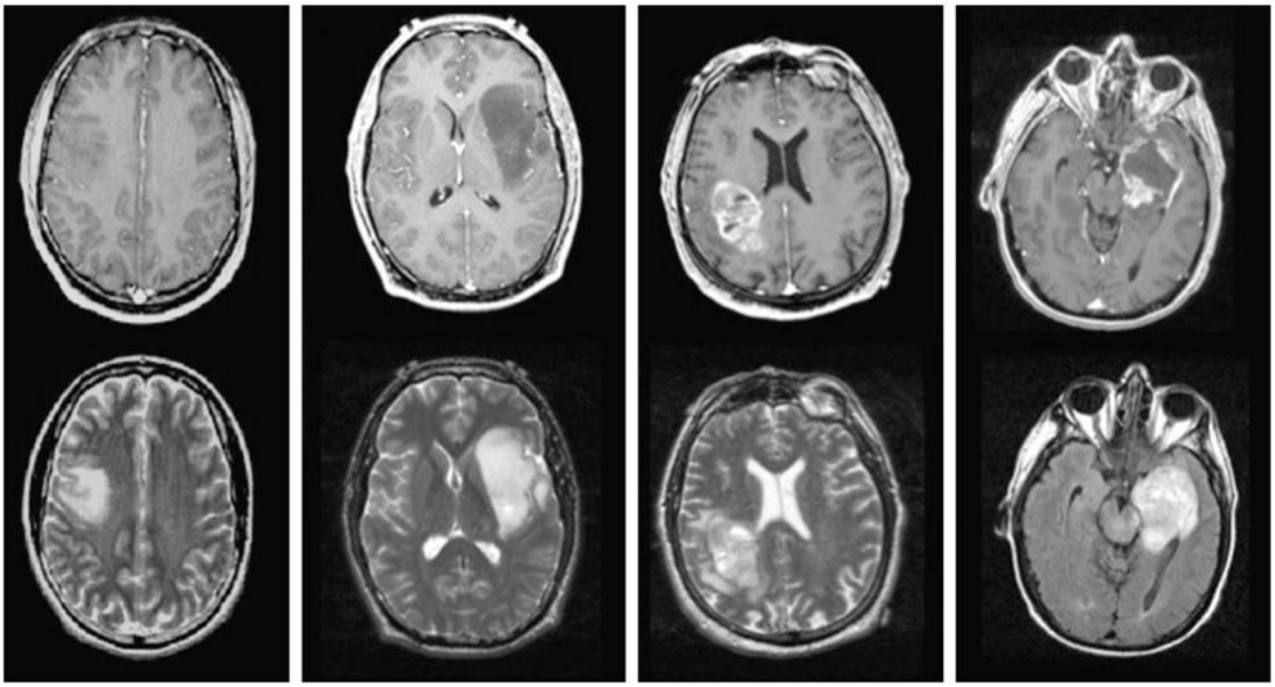

Figure 1.
Post-gadolinium T_1-weighted and T_2-weighted images from patients with grade II astrocytoma (left), grade III anaplastic astrocytoma (middle left), glioblastoma multiforme (GBM) with heterogeneous enhancement (middle right) and GBM with central necrosis (right).

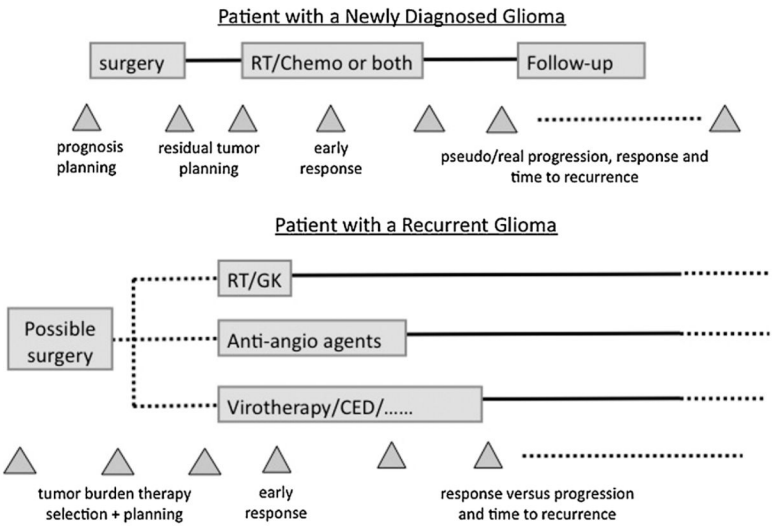

Figure 2.

Treatment schema for patients with glioma showing the time points at which imaging is used to plan surgery and radiation therapy (RT), to assess tumor burden and to evaluate the response to therapy. CED, convection-enhanced delivery; GK, gamma knife.

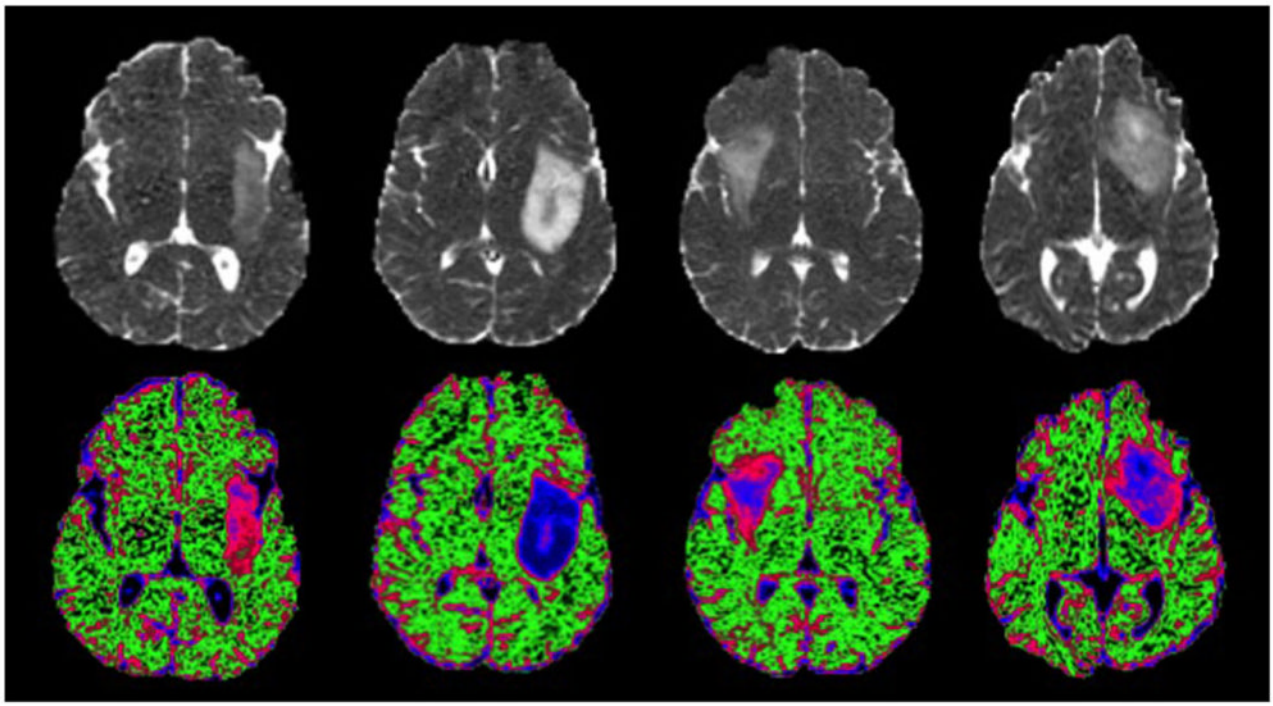

Figure 3.
Apparent diffusion coefficient (ADC) images and color-coded maps demonstrating differences in ADC values between patients with oligodendroglioma (far left), astrocytoma (mid-left) and two patients with mixed histology that was classified as oligoastrocytoma (mid-right and far right). The color maps highlight the regions with ADC values that are characteristic of normal brain (green), oligodendroglioma (pink) and astrocytoma (blue). Note the variable spatial patterns of color intensity in the lesions with mixed histology.

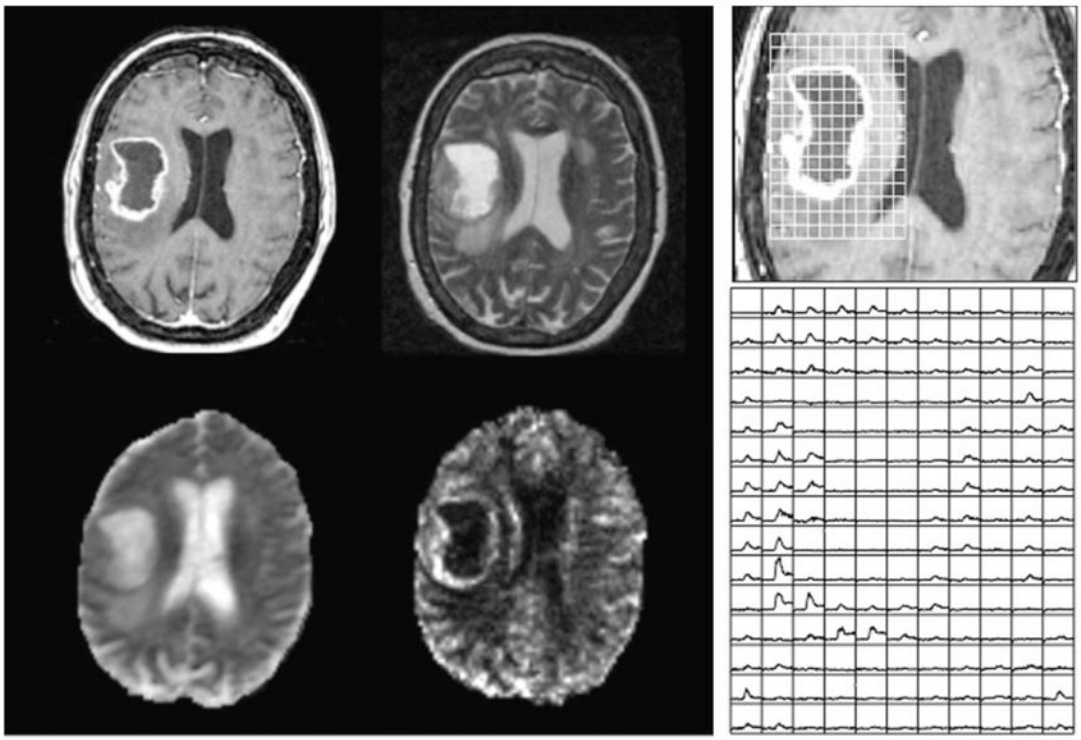

Figure 4.
Post-gadolinium T_1-weighted (top left), T_2-weighted (top right), apparent diffusion coefficient (ADC) (bottom left) and normalized cerebral blood volume (nCBV) (bottom right) images from a patient with an untreated glioblastoma multiforme (GBM). The panel on the right shows the dynamic curves from the dynamic susceptibility-weighted contrast (DSC) data in a region corresponding to the lesion, illustrating the lack of signal in the necrotic core, as well as increased nCBV and reduced recovery in areas of the enhancing rim.

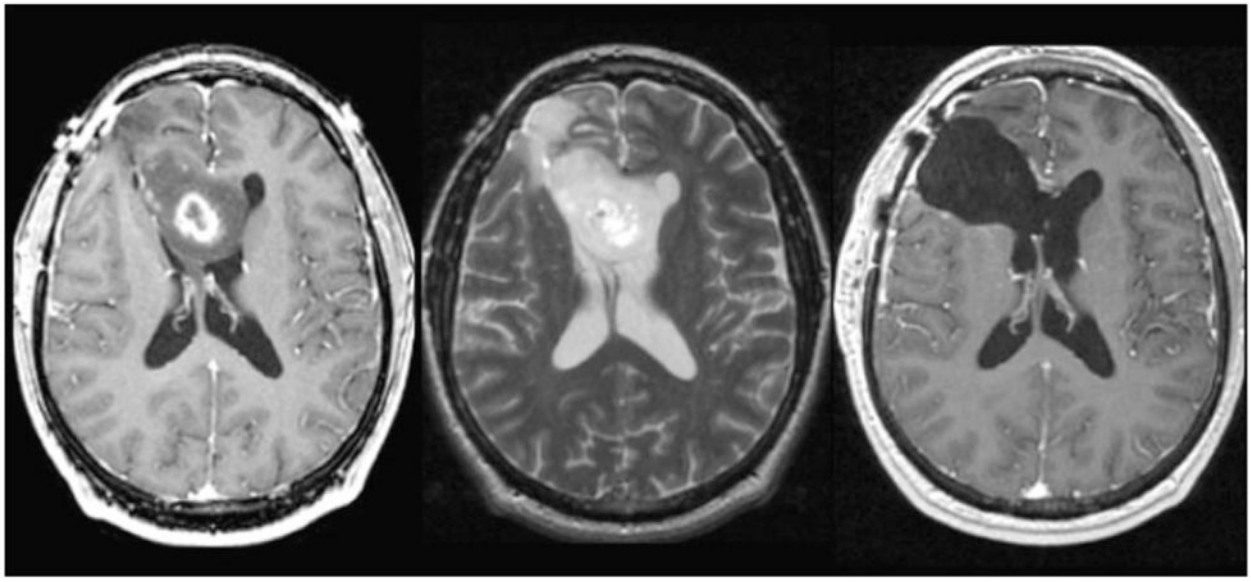

Figure 5.
Patient with a large glioblastoma multiforme (GBM) prior to surgery (left and middle), but showing an extensive resection with no enhancing tumor on the post-gadolinium T_1-weighted image (right). Although this is an excellent outcome for the patient, it means that conventional methods for assessing the response to therapy cannot be used to assess the response to further treatment because they are referenced to the size of the residual enhancing tumor.

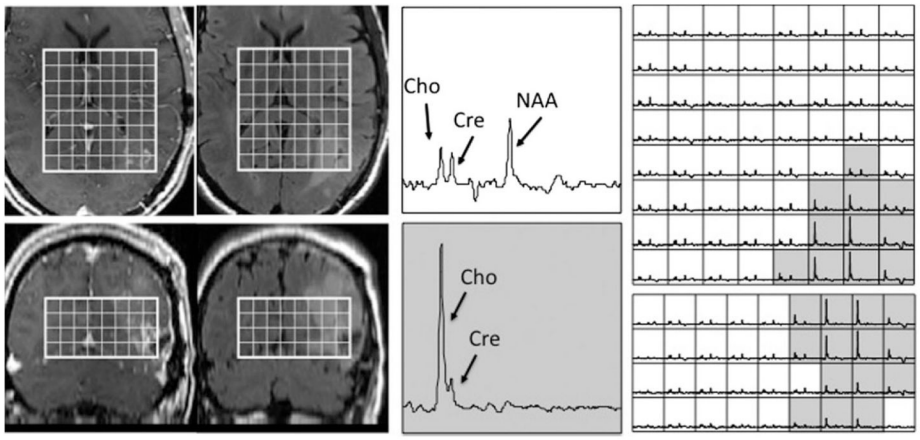

Figure 6.

Patient with a newly diagnosed glioblastoma multiforme (GBM) who had an extensive resection that left limited enhancing tumor on the post-gadolinium T_1-weighted axial and coronal images (left), but for which there was a large residual metabolic lesion (as seen from the voxels shaded in gray) that corresponded to elevated but intermediate signal intensity on the fluid-attenuated inversion recovery (FLAIR) images (right). The two enlarged spectra in the middle panel show the differences in specific metabolites and correspond to normal brain (top) and tumor (below). The MRSI data were acquired at 1.5 T using a point-resolved spectroscopy (PRESS) localization and three-dimensional phase encoding with out-of-voxel suppression pulses, TR/TE =1000/144ms, elliptical *k*-space sampling, 12 × 12 × 8 matrix and 120 × 120 × 80 mm^3 field of view. Cho, choline-containing compounds; Cre, creatine; NAA, *N*-acetylaspartate.

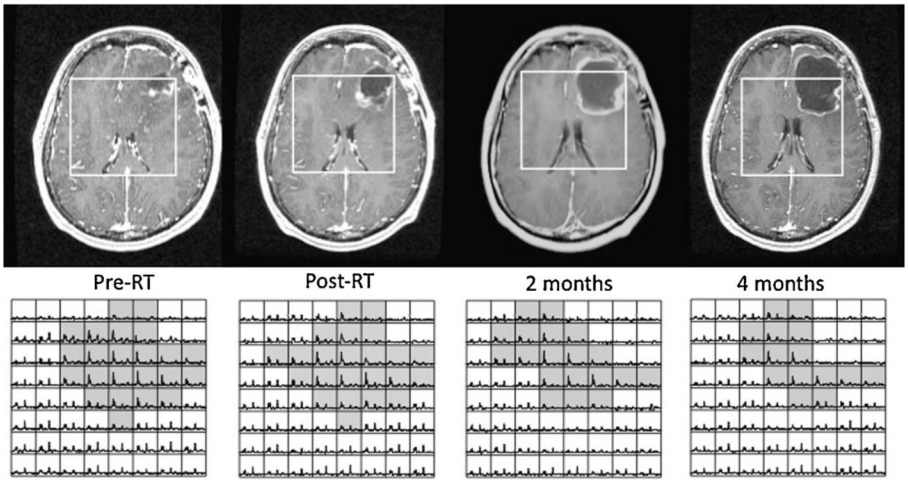

Figure 7.

Changes in post-gadolinium T_1-weighted images and MRSI data for a patient with a newly diagnosed glioblastoma multiforme (GBM) who was treated with external beam radiation therapy. The voxels shaded in gray have elevated choline to *N*-acetylaspartate (NAA) relative to normal brain and correspond mainly to nonenhancing tumor. Note that the changes in enhancement are ambiguous, but that there is a steady overall decrease in the size of the metabolic lesion. RT, radiation therapy.

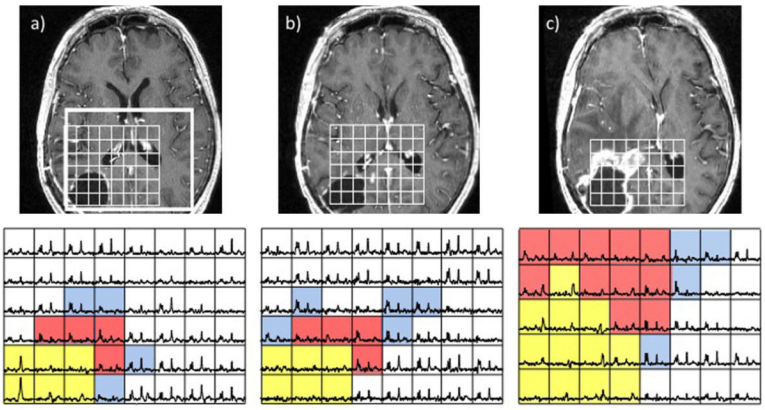

Figure 8.

Serial post-gadolinium T_1-weighted images (top) and MRSI data (bottom) from a patient with a newly diagnosed glioblastoma multiforme (GBM) post-surgery and pre-radiation therapy (RT) (a), post-RT when there was no change in enhancement but some areas of hyperintensity around the cavity on the corresponding fluid-attenuated inversion recovery (FLAIR) image (b) and 4 months after RT with a clear increase in the size of the lesion (c). The blue voxels show elevated choline to *N*-acetylaspartate (NAA), the red voxels show both elevated choline to NAA and some lactate/lipid peaks, and the yellow voxels, which are initially in the surgical cavity and then extend into the new gadolinium-enhancing lesion, show elevated lactate/lipid peaks but no choline, creatine or NAA. Note that the metabolic lesion showed clear evidence of residual and expanding tumor prior to the change in gadolinium enhancement.

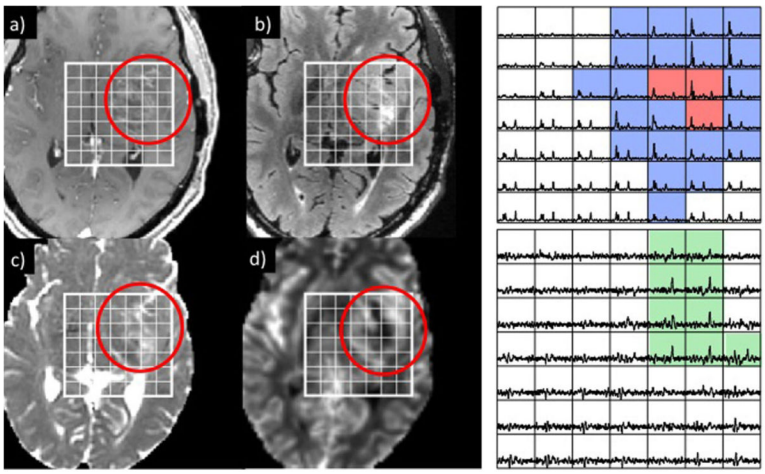

Figure 9.

Post-gadolinium T_1-weighted (a), fluid-attenuated inversion recovery (FLAIR) (b), apparent diffusion coefficient (ADC) (c) and relative cerebral blood volume (rCBV) (d) images from a region of suspected recurrence in a patient who was originally diagnosed with a grade II astrocytoma. Despite the relatively mild degree of enhancement on the T_1 image, there was elevated rCBV in the rim of the lesion, as well as significant regions of abnormal metabolism on the lactate-edited MRSI data. The spectra in the top array show peaks corresponding to elevated choline to *N*-acetylaspartate (NAA) with no lipid (blue) and both elevated choline to NAA and lipid (red), whereas the bottom array (scaled up by a factor of three) shows peaks corresponding to lactate (green). The patient went for surgery and was diagnosed as having upgraded to a glioblastoma multiforme (GBM).

Table 1

Relationship between MR parameters and biological properties of the tumor that can be obtained by quantitative analysis of the proposed multiparametric imaging examination for patients with glioma

Biological process	MR techniques	MR parameters
Invasion	DTI, ^{1}H MRSI	Reduced NAA, reduced FA, increased ADC
Tumor cellularity	DTI, ^{1}H MRSI	Decreased ADC, increased Cho, increased CNI
Proliferation	^{1}H MRSI	Increased Cho, increased CNI
Apoptosis/necrosis	^{1}H MRSI	Increased lipid
Hypoxia	Lactate-edited ^{1}H MRSI, hyperpolarized ^{13}C imaging	Increased lactate
Gliosis	Short echo ^{1}H MRSI	Increased myo-inositol/Cho
Edema	DTI	Highly increased ADC, reduced FA
Angiogenesis	DCE or DSC imaging	Increased rCBV or fBV, changes in K_{trans} or %REC
Late RT effects	SWI	Appearance of micro-hemorrhages

ADC, apparent diffusion coefficient; Cho, choline-containing compounds; CNI, choline to *N*-acetylaspartate index; DCE, dynamic contrast-enhanced; DSC, dynamic susceptibility-weighted contrast; DTI, diffusion tensor imaging; FA, fractional anisotropy; fBV, fractional blood volume; K_{trans}, fitted constant describing leakage of the contrast agent into the interstitial space; NAA, *N*-acetylaspartate; rCBV, relative cerebral blood volume; %REC, percentage recovery of the DSC signal to baseline; RT, radiation therapy; SWI, susceptibility-weighted imaging.